SIAM J. Applied Dynamical Systems
Vol. 16, No. 3, pp. 1260–1308

Swarm Equilibria in Domains with Boundaries*

R. C. Fetecau† and M. Kovacic†

Abstract. We study equilibria in domains with boundaries for a first-order aggregation model that includes social interactions and exogenous forces. Such equilibrium solutions can be connected or disconnected, the latter consisting in a delta concentration on the boundary and a free swarm component in the interior of the domain. Equilibria are stationary points of an energy functional, and stable configurations are local minimizers of this functional. We find a one-parameter family of disconnected equilibrium configurations which are not energy minimizers; the only stable equilibria are the connected states. Nevertheless, we demonstrate that in certain cases the dynamical evolution, along the gradient flow of the energy functional, tends to overwhelmingly favor the formation of (unstable) disconnected equilibria.

Key words. swarm equilibria, energy minimizers, gradient flow, attractors, nonsmooth dynamics

AMS subject classifications. 35A15, 35Q92, 45B05, 45K05, 70K20

DOI. 10.1137/17M1123900

1. Introduction.

Research in mathematical modelling for self-organizing behavior or swarming has surged in recent years. An aggregation model that has attracted a great amount of interest is given by the following integro-differential equation in $\mathbb{R}^n$:

$$\rho_t + \nabla \cdot (\rho v) = 0, \tag{1a}$$

$$v = -\nabla K * \rho - \nabla V. \tag{1b}$$

Here ρ represents the density of the aggregation, K is an interaction potential, and V is an external potential. The asterisk $(*)$ denotes convolution. Typically, the interaction potential K models symmetric interindividual social interactions such as long-range attraction and short-range repulsion.

Model (1) appears in various contexts related to swarming and social aggregations, and the associated literature is vast, covering a wide range of topics: modelling and pattern formation [36, 41, 34, 35, 27], well-posedness of solutions [12, 9, 8], long time behavior of solutions [26, 35], and blowup (in finite or infinite time) by mass concentration [25, 8, 32]. The equation also arises in a number of other applications such as granular media [43, 17], self-assembly of nanoparticles [30, 31], Ginzburg–Landau vortices [23, 22], molecular dynamics simulations of matter [29], and opinion dynamics [37].

In this paper we study the aggregation model (1) in domains with boundaries. Despite the extensive literature on model (1) in free space, there has been only a handful of works

*Received by the editors August 10, 2016; accepted for publication (in revised form) by B. Sandstede April 8, 2017; published electronically July 12, 2017.
http://www.siam.org/journals/siads/16-3/M112390.html
Funding: The first author was supported during this research by NSERC Discovery Grant PIN-341834.
†Department of Mathematics, Simon Fraser University, 8888 University Dr., Burnaby, BC, V5A 1S6, Canada (van@math.sfu.ca, mkovacic@sfu.ca).

that consider the presence of boundaries [7, 44, 18]. These papers are motivated by physical/biological scenarios where the environment involves an obstacle or an impenetrable wall; in the locust model from [42], for example, such an obstacle is the ground. We assume in this work that the presence of boundaries limits the movement in the following way [44, 18]: Once particles/individuals meet the boundary, they do not exit the domain but instead move freely along it. The precise mathematical formalism of this "slip, no-flux" boundary condition is elaborated below.

Consider the aggregation model (1) confined to a closed domain $\Omega \subset \mathbb{R}^n$. Suppose that Ω has a smooth C^1 boundary with outward normal vector ν_x at $x \in \partial\Omega$. The geometric confinement constrains the velocity field as follows: At points in the interior of Ω, or at points on the boundary where the velocity vector, computed with (1b), points inward ($v \cdot \nu_x \leq 0$), no modification is needed, and the velocity is given by (1b). On the other hand, for points on the boundary where the velocity computed with (1b) points *outward* ($v \cdot \nu_x > 0$), its projection on the tangent plane to the boundary is considered instead.

The model in domains with boundaries is then given by

$$\rho_t + \nabla \cdot (\rho v) = 0, \tag{2a}$$

$$v = P_x(-\nabla K * \rho - \nabla V), \tag{2b}$$

where

$$P_x\xi = \begin{cases} \xi & \text{if } x \notin \partial\Omega \ \text{ or } \ x \in \partial\Omega \text{ and } \xi \cdot \nu_x \leq 0, \\ \Pi_{\partial\Omega}\,\xi & \text{otherwise.} \end{cases} \tag{3}$$

Here $\Pi_{\partial\Omega}$ denotes the projection on the tangent plane to the boundary. Note that solutions to (2) conserve the total mass; however, the linear momentum is no longer preserved (as opposed to the model in free space). The latter observation has important implications for the long time behavior of the solutions, as discussed later in the paper.

The well-posedness of weak measure solutions of (2) has been investigated recently in [44, 18] in the framework of gradient flows in spaces of probability measures [1, 16]. The setting of *measure*-valued solutions in these works is absolutely essential in this context, for various reasons. First, mass accumulates on the boundary of the domain, and solutions develop Dirac delta singularities there. Second, the measure framework is the appropriate setup for connecting the PDE model with its discrete/particle approximation. In regard to the latter, by approximating the initial density ρ_0 with a finite number of delta masses, (2) reduces to an ODE system, which then can be studied on its own. In [18], the authors establish several important properties of such particle approximations. One is the well-posedness of the approximating particle system where, due to the discontinuities of the velocity field at the boundary, the theory of differential inclusions [28, 21] is being employed. Another is the rigorous limit of the discrete approximation as the number of particles approaches infinity; this limit is shown to be a weak measure solution of the PDE model (2).

The focus of the present paper is equilibrium configurations of model (2). A density $\bar{\rho}$ is an equilibrium if the velocity (2b) vanishes everywhere on its support:

$$P_x(-\nabla K * \bar{\rho} - \nabla V) = 0 \qquad \text{in } \operatorname{supp}(\bar{\rho}). \tag{4}$$

We note, however, that at points on the boundary, the unprojected velocity (i.e., $-\nabla K * \bar{\rho} - \nabla V$) may not be zero; by (3) it can have a nonzero normal component that is pointing outward. This scenario is akin to a falling object hitting a surface, when there is still a force acting on it, but there is nowhere to go.

Model (2) is a gradient flow, and its equilibria are stationary points of the energy functional. We use the framework developed by Bernoff and Topaz [7] to look for these stationary densities. We also investigate their stability; given the variational formulation, stable equilibria can be characterized as local minima of the energy. Most of the paper concerns a specific interaction potential, consisting of Newtonian repulsion and quadratic attraction [27, 26]. The main advantage of using this potential is that the equilibria must have constant densities away from the boundary, which restricts the possible equilibrium configurations and simplifies the calculations.

The present paper contains the first systematic study of equilibria for model (2) in two dimensions; we note here that the results in [7] consider only cases in one and quasi-two dimensions. Of particular relevance is a family of two-component equilibria that we found in our study (in both one and two dimensions), consisting of one swarm component on the boundary and another in the interior of the domain. These two-component equilibria can be further differentiated as connected or disconnected, depending on whether the two components are adjacent or not. We find that none of the disconnected equilibria are local minima of the energy. In contrast, some connected configurations can be shown to be local (and in some cases global) energy minimizers.

Nevertheless, we show that starting from a large class of initial densities, solutions to (2) do evolve into such (unstable) disconnected equilibria that are not local energy minimizers. While unusual, this behavior has been observed in continuum mechanics systems wherein singularities form which act as barriers preventing further energy decrease [4, 5, 40]. Describing and understanding this behavior for model (2) is one of the main goals of this paper.

The summary of the paper is as follows. Section 2 presents some background on model (2). In section 3 we study the one-dimensional problem on a half-line. We find explicit expressions for the equilibria and make various investigations of the dynamical model to quantify how these equilibria are being reached. Section 4 considers the two-dimensional problem on a half-plane. We compute the connected and disconnected equilibria and investigate their stability. Finally, we present details on the numerical implementations.

2. Preliminaries.

Well-posedness and gradient flow formulation. The well-posedness of weak measure solutions to model (2) has been established recently in [44] and [18]. The functional setup in these works consists in the space $\mathcal{P}_2(\Omega)$ of probability measures on Ω with finite second moment, endowed with the 2-Wasserstein metric. Under appropriate assumptions on the domain Ω and on the potentials K and V, it is shown that the initial value problem for (2) admits a weak measure solution $\rho(t)$ in $\mathcal{P}_2(\Omega)$. We refer the reader to [44, 18] for specific details on the well-posedness theorems and proofs; here we highlight only the facts that are relevant for our work.

It is a well-established result that the aggregation model in free space (model (1)) can be formulated as a gradient flow on the space of probability measures $\mathcal{P}_2(\Omega)$ equipped with the 2-Wasserstein metric [1]. A key result in [44, 18] is that such an interpretation exists for

model (2) as well. Specifically, consider the energy functional

$$E[\rho] = \frac{1}{2}\int_\Omega\int_\Omega K(x-y)\rho(x)\rho(y)\,dx\,dy + \int_\Omega V(x)\rho(x)\,dx, \tag{5}$$

where the first term represents the interaction energy and the second is the potential energy.[1]

The weak measure solution $\rho(x,t)$ to model (2) is shown to satisfy the following energy dissipation equality [18]:

$$E[\rho(t)] - E[\rho(s)] = -\int_s^t\int_\Omega |P_x(-\nabla K * \rho(x,\tau) - \nabla V(x))|^2\rho(x,\tau)\,dx \tag{6}$$

for all $0 \le s \le t < \infty$. Equation (6) is a generalization of the energy dissipation for the model in free space [16]. Characterization of equilibria of (1) as ground states of the interaction energy (5) has been a very active area of research lately [2, 20, 14, 38].

The authors in [18] use particle approximations of the continuum model (2) as an essential tool to show the existence of gradient flow solutions. The method consists in approximating an initial density ρ_0 by a sequence ρ_0^N of delta masses supported at a discrete set of points. For N fixed, the evolution of model (2) with discrete initial data ρ_0^N reduces to a system of ODEs, for which ODE theory can be applied. The ODE system governs the evolution of the characteristic paths (or particle trajectories) which originate from the points in the discrete support of ρ_0^N. Hence, the solution $\rho^N(t)$ consists of delta masses supported at a discrete set of characteristic paths. The key ingredient in the analysis is to find a stability property of solutions ρ^N with respect to initial data ρ_0^N and show that in the limit $N \to \infty$, ρ^N converges (in the Wasserstein distance) to a weak measure solution of (2) with initial data ρ_0. This is one of the major results established in [18].

Equilibria and energy minimizers. The authors in [7] study the energy functional (5) and find conditions for critical points to be energy minimizers. We briefly review the setup there.

First note that the dynamics of model (2) conserves mass:

$$\int_\Omega \rho(x,t)\,dx = M \qquad \text{for all } t \ge 0. \tag{7}$$

Hence, in what follows it is sufficient to consider zero-mass perturbations of a fixed equilibrium.

Single-component equilibria. Consider an equilibrium solution $\bar\rho$ with mass M and *connected* support $\Omega_{\bar\rho} \subset \Omega$, and take a small perturbation $\epsilon\tilde\rho$ of zero mass:

$$\rho(x) = \bar\rho(x) + \epsilon\tilde\rho(x),$$

where

$$\int_\Omega \bar\rho(x)\,dx = M, \tag{8a}$$

$$\int_\Omega \tilde\rho(x)\,dx = 0. \tag{8b}$$

[1] Note that throughout the present paper $\int \varphi(x)\rho(x)\,dx$ denotes the integral of φ with respect to the measure ρ, regardless of whether ρ is absolutely continuous with respect to the Lebesgue measure.

Since the energy functional is quadratic in ρ, one can write

$$E[\rho] = E[\bar{\rho}] + \epsilon E_1[\bar{\rho}, \tilde{\rho}] + \epsilon^2 E_2[\tilde{\rho}, \tilde{\rho}],$$

where E_1 denotes the first variation,

$$E_1[\bar{\rho}, \tilde{\rho}] = \int_\Omega \left[\int_\Omega K(x-y)\bar{\rho}(y)\,\mathrm{d}y + V(x) \right] \tilde{\rho}(x)\,\mathrm{d}x, \tag{9}$$

and E_2 denotes the second variation,

$$E_2[\tilde{\rho}, \tilde{\rho}] = \frac{1}{2} \int_\Omega \int_\Omega K(x-y)\tilde{\rho}(x)\tilde{\rho}(y)\,\mathrm{d}x\,\mathrm{d}y. \tag{10}$$

Using the notation

$$\Lambda(x) = \int_{\Omega_{\bar{\rho}}} K(x-y)\bar{\rho}(y)\,\mathrm{d}y + V(x) \qquad \text{for } x \in \Omega, \tag{11}$$

one can also write the first variation as

$$E_1[\bar{\rho}, \tilde{\rho}] = \int_\Omega \Lambda(x)\tilde{\rho}(x)\,\mathrm{d}x. \tag{12}$$

Two classes of perturbations are considered in [7]: perturbations $\tilde{\rho}$ supported in $\Omega_{\bar{\rho}}$ (first class), and general perturbations $\tilde{\rho}$ in the domain Ω (second class). Perturbations of the first class are a subset of the perturbations of the second class.

Start by taking perturbations of the first class. Since $\tilde{\rho}$ changes sign in $\Omega_{\bar{\rho}}$, for $\bar{\rho}$ to be a critical point of the energy, the first variation must vanish. From (12), given that perturbations $\tilde{\rho}$ are arbitrary and satisfy (8b), one finds that E_1 vanishes, provided that Λ is constant in $\Omega_{\bar{\rho}}$, i.e.,

$$\Lambda(x) = \lambda \qquad \text{for } x \in \Omega_{\bar{\rho}}. \tag{13}$$

The (Lagrange) multiplier λ is given a physical interpretation in [7]: It represents the energy per unit mass felt by a test mass at position x due to interaction with the swarm in $\bar{\rho}$ and the exogenous potential. Indeed this interpretation is valid for all points x by considering $\Lambda(x)$ as the energy per unit mass felt by a test mass at position x. This interpretation is critical for the study in [7], as well as for the present paper.

Equation (13) represents a necessary condition for $\bar{\rho}$ to be an equilibrium. For $\bar{\rho}$ that satisfies (13) to be a local minimizer with respect to the first class of perturbations, the second variation (10) must be positive. In general, the sign of E_2 cannot be easily assessed.

Now consider perturbations of the second class. Since perturbations $\tilde{\rho}$ must be nonnegative in the complement $\Omega_{\bar{\rho}}^c = \Omega \setminus \Omega_{\bar{\rho}}$, it is shown in [7] that a necessary and sufficient condition for $E_1 \geq 0$ is

$$\Lambda(x) \geq \lambda \qquad \text{for } x \in \Omega_{\bar{\rho}}^c. \tag{14}$$

The interpretation of (14) is that transporting mass from $\Omega_{\bar\rho}$ into its complement $\Omega_{\bar\rho}^c$ increases the total energy [7].

In summary, a critical point $\bar\rho$ for the energy satisfies the Fredholm integral equation (13) on its support. Also, $\bar\rho$ is a local minimizer (with respect to the general, second class perturbations) if it satisfies (14). Note, however, that the word *local* in this context refers to the small *size* of the perturbations, as the perturbations themselves are in fact allowed to be nonlocal in space.

Remark 2.1 (formal variational framework). The minimization considerations above closely follow the *informal* setup and approach from [7]; for a mathematically complete and rigorous framework one needs to be more precise, however. First, one has to set the space of densities over which the minimization of energy is considered (i.e., the space to which the equilibrium $\bar\rho$ and the perturbed equilibrium ρ belong). We take the space of such admissible densities to be the set of Borel measures on Ω that have finite second moment and total mass M, endowed with the 2-Wasserstein metric. Apart from not having a density normalized to unit mass (which does not add any technical difficulties), this is the framework commonly used in rigorous variational studies of model (1) [2, 3, 16], including the recent work on domains with boundaries [44, 18].

A rigorous derivation of the Euler–Lagrange equations within such a formal setup is presented, for instance, in [2, Theorem 4]; note that while the derivation there is for equilibria in free space, it extends immediately to arbitrary domains Ω, as considered in this paper. As in [2], by considering various types of admissible perturbations to an equilibrium $\bar\rho$ (similar in fact to the first and second class perturbations from [7]), one finds that (13) holds a.e. (with respect to the measure $\bar\rho$) within the support, while (14) holds at a.e. x. Hence, the necessary conditions (13) and (14) for a local minimum, as found through the informal approach in [7], could potentially be relaxed by requiring them to hold up to zero measure sets. Nevertheless, given the connected equilibria considered in this paper, working directly with (13) and (14) is simpler and makes no essential difference in our considerations.

Multicomponent equilibria. As discussed in [7], the support $\Omega_{\bar\rho}$ of an equilibrium density has in general multiple disconnected components. Assuming m disjoint, closed, and connected components Ω_i, $i = 1, \dots, m$, one can write

$$\Omega_{\bar\rho} = \Omega_1 \cup \Omega_2 \cup \cdots \cup \Omega_m, \qquad \Omega_i \cap \Omega_j = \emptyset, \quad i \neq j. \tag{15}$$

In [7], a *swarm equilibrium* is defined as a configuration in which Λ is constant in every component of the swarm, i.e.,

$$\Lambda(x) = \lambda_i \qquad \text{for } x \in \Omega_i, \quad i = 1, \dots, m. \tag{16}$$

Remark 2.2. We first point out that condition (16) is only a *necessary* condition for $\bar\rho$ to be an equilibrium of (2). Indeed, consider a density $\bar\rho$ that satisfies (16), and check whether it satisfies the equilibrium condition (4). By (16), (4) is indeed satisfied in every component Ω_i that lies in the interior of Ω (the projection plays no role there). However, consider a component Ω_i of the swarm that lies *on* the boundary of the physical domain Ω. The component Ω_i can be, for instance, a codimension one manifold, such as a line in $\mathbb{R}^2$; in fact,

our numerical investigations in section 4 focus on this example. Since $\Lambda(x)$ is constant on $\Omega_i \subset \partial\Omega$, we infer that the tangential component to $\partial\Omega$ of $\nabla\Lambda$ is zero at any point $x \in \Omega_i$. Consequently, by (11), we conclude that the unprojected velocity at x (cf. (1b)) is *normal* to $\partial\Omega$. For an equilibrium solution, this normal component must point *into* $\partial\Omega$ ($v \cdot \nu_x > 0$) (see (2b) and (3)); however, one cannot infer this condition from (16). Section 4 provides examples where solutions to (16) do not yield equilibria, precisely because the velocity at some points on the boundary is directed toward the interior of Ω, and thus the steady state condition (4) fails.

Given the physical interpretation of $\Lambda(x)$, one can immediately observe that a multicomponent equilibrium $\bar{\rho}$ that satisfies (16) cannot be a local minimizer unless all λ_i are equal to each other ($i = 1, \dots, m$). Indeed, for a swarm equilibrium with $\lambda_j > \lambda_k$, transferring mass from Ω_j to Ω_k would decrease the energy. In the applications considered in this paper, we have not identified a disconnected equilibrium with a common value for $\Lambda(x)$ in each component of the support. We have, however, identified families of two-component equilibria that satisfy (16) with $\lambda_1 \neq \lambda_2$. While such equilibria cannot be minimizers with respect to arbitrary perturbations, we investigate instead whether such equilibria are minimizers with respect to perturbations that are *local in space* [7].

Following [7], we define a *swarm minimizer* as a swarm equilibrium which satisfies

$$\Lambda(x) \geq \lambda_i \qquad \text{in some neighborhood of each } \Omega_i. \tag{17}$$

By the interpretation of Λ, (17) means that an infinitesimal redistribution of mass in a neighborhood of Ω_i increases the energy.

Remark 2.3 (locality of perturbations). The word "local" has appeared above in various instances with very different meanings. In the phrase "local minimizer," the word *local* refers to the small *size* of the perturbations. On the other hand, for a multicomponent swarm minimizer, (17) has to hold only in a *neighborhood* of each component, which indicates that only perturbations $\tilde{\rho}$ that are *local in space* are considered. In other words, a swarm minimizer is a *local minimizer* of the energy with respect to admissible perturbations $\epsilon\tilde{\rho}$ that are *local in space* (for precise terminology and a formal variational setup, see Remark 2.1).

Multicomponent equilibria of model (2) are a major focus of the present study. To find such equilibria we look for solutions of (16), and then we check (17) to decide whether the equilibria are swarm minimizers. In sections 3 and 4 we investigate two-component swarm equilibria in both one and two dimensions. For all such equilibria, $\lambda_1 \neq \lambda_2$; in fact, the two components of the support approach each other (and hence become a connected equilibrium) as λ_1 and λ_2 approach a common value.

Newtonian repulsion and quadratic attraction. The present study focuses on a specific interaction potential K given by

$$K(x) = \phi(x) + \frac{1}{2}|x|^2, \tag{18}$$

where $\phi(x)$ is the free-space Green's function for the negative Laplace operator $-\Delta$:

$$\phi(x) = \begin{cases} -\frac{1}{2}|x|, & n = 1, \\ -\frac{1}{2\pi}\ln|x|, & n = 2. \end{cases} \tag{19}$$

Potentials in the form (18), consisting of Newtonian repulsion and quadratic attraction, have been considered in various recent works [25, 27, 26, 33]. The remarkable property of such potentials is that they lead to compactly supported equilibrium states of constant densities [25, 27]. This property will be further elaborated below.

We note that the analysis in [44, 18] requires assumptions on K which the potential (18) does not satisfy. In particular, in that analysis, the interaction potential is required to be C^1 and λ-geodesically convex. Consequently, the results in [44, 18] do not immediately apply to our study. Nevertheless we consider the framework developed in these papers, in particular, the gradient flow and the energy dissipation (see (6)), and the particle approximation method which can be turned into a very valuable computational tool. Indeed, to validate our equilibrium calculations we use a particle method to simulate solutions to (2).

Equilibria corresponding to potential (18). In the absence of an exogenous potential ($V = 0$), the aggregation model (1) with interaction potential (18) evolves into constant, compactly supported steady states. This can be inferred from a direct calculation using the specific form of the potential (18). Indeed, expand

$$\nabla \cdot (\rho v) = v \cdot \nabla \rho + \rho \nabla \cdot v,$$

and write the aggregation equation (1) as

$$\rho_t + v \cdot \nabla \rho = -\rho \nabla \cdot v. \tag{20}$$

From (1b) and (18), using $-\Delta \phi = \delta$ and the mass constraint (7), one gets

$$\begin{aligned} \nabla \cdot v &= -\Delta K * \rho \\ &= \rho - nM. \end{aligned} \tag{21}$$

This calculation shows that $\nabla \cdot v$ is a *local* quantity. By using (21) in (20), one finds that along characteristic paths $X(\alpha, t)$, defined by

$$\frac{d}{dt} X(\alpha, t) = v(X(\alpha, t), t), \qquad X(\alpha, 0) = \alpha, \tag{22}$$

$\rho(X(\alpha, t), t)$ satisfies

$$\frac{D}{Dt} \rho = -\rho(\rho - nM). \tag{23}$$

The remarkable property of the interaction potential (18), as seen from (23), is that the evolution of the density along a certain characteristic path $X(\alpha, t)$ satisfies a decoupled, stand-alone ODE. Hence, as inferred from (23), $\rho(X(\alpha, t), t)$ approaches the value nM as $t \to \infty$, along *all* characteristic paths $X(\alpha, t)$ that transport nonzero densities. More specifically, it has been demonstrated in [10, 27] that solutions to (1), with K given by (18), approach asymptotically a radially symmetric equilibrium that consists of a ball of constant density nM.

In domains with boundaries, as the velocity is projected (cf. (2b) and (3)) at points on the boundary, the characteristic equations (and the evolution of the density along characteristic

paths) should be considered in an extended, more general setup. In [18], for instance, the authors study particle approximations for model (2) within the framework of differential inclusions. We do not pursue here the idea of studying the characteristic equations for domains with boundaries. As the next calculation shows, for the purpose of this paper, which is focused on equilibria, such extension is not in fact needed.

Indeed, consider an equilibrium solution $\bar{\rho}$ of model (2) that consists of a delta accumulation on the boundary and one or several swarms in the interior of the domain. Note that, unlike the problem in free space, the interior swarms are not expected to be radially symmetric. At any point x in the support of $\bar{\rho}$, the velocity $\bar{v}$ vanishes:

$$\bar{v} = P_x(-\nabla K * \bar{\rho}) = 0.$$

In particular, at an arbitrary point x in one of the interior swarms, one has $\nabla \cdot \bar{v} = 0$, and hence, by a calculation similar to (21), one concludes that

$$\bar{\rho}(x) = nM \qquad \text{at any } x \in \operatorname{supp}(\bar{\rho}) \cap \operatorname{int}(\Omega). \tag{24}$$

This key observation is used in sections 3 and 4 to investigate equilibria for model (2).

Finally, in the presence of an external potential, calculation of $\nabla \cdot v$ from (1b) and (18) (see also (21)) yields

$$\nabla \cdot v = \rho - nM - \Delta V.$$

Following similar considerations, for an equilibrium $\bar{\rho}$ of model (2), one has

$$\bar{\rho}(x) = nM + \Delta V \qquad \text{at any } x \in \operatorname{supp}(\bar{\rho}) \cap \operatorname{int}(\Omega). \tag{25}$$

In sections 3 and 4 we work with a linear gravitational potential V for which $\Delta V = 0$, so in fact, all equilibria we consider in this paper have constant densities in the interior of the domain.

3. One dimension: Equilibria on a half-line.

In sections 3.1–3.3 we consider the one-dimensional problem on $\Omega = [0, \infty)$, with interaction kernel given by (18) and (19). In section 3.4 we consider a different interaction kernel, namely a Morse-type kernel as investigated in [7]. We study the existence and stability of both connected and disconnected equilibria throughout.

3.1. No exogenous potential.

We consider first the case $V(x) = 0$ (no exogenous forces). By (24), an equilibrium has constant density M in the part of the support that lies in the interior of the domain. We also expect that an equilibrium can have a delta aggregation buildup at the boundary [7].

Based on these considerations (see also Remark 3.2 below), we look for equilibria in the form of a delta accumulation of strength S at the origin and a constant density M in an interval $(d_1, d_1 + d_2)$, with $d_1 \geq 0$, $d_2 > 0$:

$$\bar{\rho}(x) = S\delta(x) + M\mathbb{1}_{(d_1, d_1+d_2)}. \tag{26}$$

The support $\Omega_{\bar{\rho}}$ of $\bar{\rho}$ consists of two (possibly disconnected) components:

$$\Omega_1 = \{0\} \quad \text{and} \quad \Omega_2 = [d_1, d_1 + d_2].$$

First observe that by the constant mass condition (8a), we have

$$S + Md_2 = M. \tag{27}$$

A necessary condition for $\bar{\rho}$ to be an equilibrium is to satisfy (16). Equation (16) is satisfied provided $\Lambda(x)$ is constant on each component of $\Omega_{\bar{\rho}}$:

$$\Lambda(0) = \lambda_1 \quad \text{and} \quad \Lambda(x) = \lambda_2 \quad \text{in } [d_1, d_1 + d_2]. \tag{28}$$

The calculation of $\Lambda(x)$ from (11) yields

$$\Lambda(x) = S\left(\frac{1}{2}x^2 - \frac{1}{2}x\right) + \int_{d_1}^{d_1+d_2} \left(\frac{1}{2}(x-y)^2 - \frac{1}{2}|x-y|\right) M dy. \tag{29}$$

For $x \in (d_1, d_1 + d_2)$, an elementary calculation of $\Lambda(x)$ gives

$$\Lambda(x) = \frac{1}{2}(S + Md_2 - M)x^2 + \frac{1}{2}\left(-S + M(2d_1 + d_2)(1 - d_2)\right)x + \frac{M}{6}(3d_1^2 d_2 + 3d_1 d_2^2 + d_2^3) - \frac{M}{4}(2d_1^2 + 2d_1 d_2 + d_2^2).$$

The second condition in (28) is satisfied only if the coefficients of x^2 and x of the polynomial above are zero. Setting the coefficient of x^2 to zero yields the mass constraint condition (27), while the coefficient of x vanishes, provided that

$$S = M(2d_1 + d_2)(1 - d_2). \tag{30}$$

Combining the two conditions (27) and (30), we arrive at

$$S = M(1 - d_2), \qquad d_1 = \frac{1 - d_2}{2}. \tag{31}$$

Hence, there is a family of solutions to (28) in the form (26) with parameter $d_2 \in (0, 1]$. Note that $d_1 + \frac{d_2}{2} = \frac{1}{2}$, implying that for all the equilibria in this family, the center of mass of the free swarm is at $\frac{1}{2}$.

By expressing everything in terms of d_2 only, Λ takes the following values on the two components Ω_1 and Ω_2 of $\Omega_{\bar{\rho}}$, respectively:

$$\lambda_1 = -\frac{M}{24}(1 - d_2)^3 + \frac{M}{8}(1 - d_2)^2 - \frac{M}{12}, \tag{32a}$$

$$\lambda_2 = -\frac{M}{24}(1 - d_2)^3 - \frac{M}{12}. \tag{32b}$$

Note that $\lambda_1 > \lambda_2$ unless $d_2 = 1$, in which case $\lambda_1 = \lambda_2$. Based on this observation, we distinguish between two qualitatively different equilibria.

(i) *Disconnected equilibria ($d_1 > 0$).* A generic disconnected solution to (28) of form (26) is shown in Figure 1(a); the solid line indicates the constant density in the free swarm, and the circle on the vertical axis indicates the strength S of the delta aggregation at the origin. Note that in *all* numerical simulations presented in this paper we take $M = 1$.

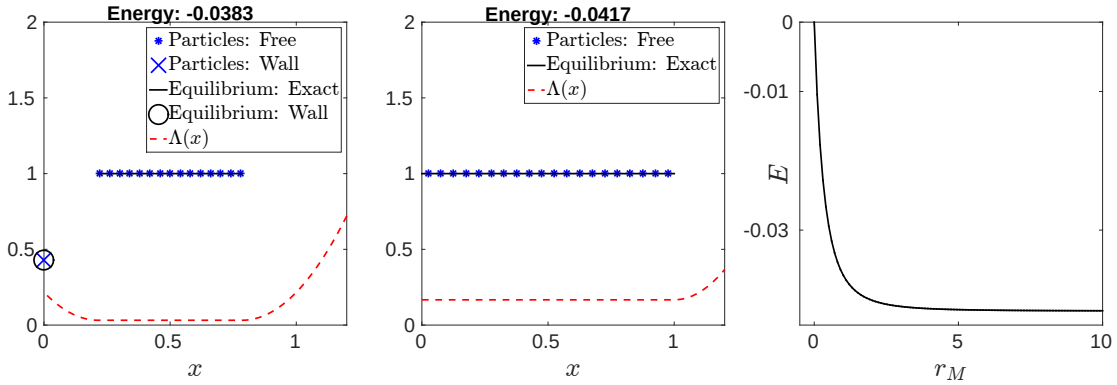

(a) (b) (c)

Figure 1. *Equilibria* (26) *on a half-line for* $V = 0$ *(no exogenous potential).* (a) *Disconnected equilibrium consisting in a free swarm of constant density and a delta aggregation at the origin.* (b) *Connected equilibrium of constant density in* $(0, 1)$. (c) *Energy of equilibria* (26) *as a function of the mass ratio; the lowest energy state corresponds to the connected equilibrium* ($r_M = \infty$). *Note that for a better visualization* $\Lambda(x)$ *has been shifted and stretched vertically.*

To check that these solutions to (28) are in fact equilibria reduces to showing that the velocity (see (2b) and (3)) vanishes at points in the support $\Omega_{\bar\rho} = \Omega_1 \cup \Omega_2$. Since $\Lambda(x)$ is constant in $[d_1, d_1 + d_2]$, it follows that the velocity vanishes everywhere in Ω_2. The more delicate part is evaluating the velocity at the origin. By (2b), the velocity at the origin is computed by accounting (via a spatial convolution) for all the attractive and repulsive effects of points that lie in $\Omega_{\bar\rho}$. The key observation is that the point at the origin (the only point in Ω_1) does not have any interaction effects on the origin itself; in a discrete setting this amounts to the fact that particles sitting on top of each other do not exert interactions (attractive or repulsive) among themselves. Therefore, the velocity $v(0)$ calculated from (2b) reduces to an integral over Ω_2 only:

$$v(0) = P_0\left(-\int_{\Omega_2} K'(-y)\bar\rho(y)dy\right). \tag{33}$$

An elementary calculation, using $K'(y) = y - \mathrm{sgn}(y)$ and $\bar\rho(y) = M$ in $\Omega_2 = (d_1, d_1 + d_2)$, yields

$$-\int_{\Omega_2} K'(-y)\bar\rho(y)dy = \frac{M}{2}d_2(2d_1 + d_2 - 1). \tag{34}$$

Finally, by (31),

$$v(0) = P_0(0) = 0,$$

so the disconnected state is indeed an equilibrium.

We now check whether the disconnected equilibria are energy minimizers. By an elementary calculation, we find from (29) (also using (31))

$$\Lambda'(x) = M(x - d_1) \quad \text{for } x \in (0, d_1) \quad \text{and} \quad \Lambda'(x) = M(x - d_1 - d_2) \quad \text{for } x \in (d_1 + d_2, \infty).$$

Consequently, for all $0 < d_2 < 1$ (or, equivalently, $0 < d_1 < \frac{1}{2}$), $\Lambda(x)$ is strictly decreasing in $(0, d_1)$ and strictly increasing in $(d_1 + d_2, \infty)$; for an illustration, see the dashed line in Figure 1(a). This calculation shows that disconnected equilibria $\bar{\rho}$ in the form (26) are *not* local minima (swarm minimizers), as (14) is not satisfied near the origin; since Λ is strictly decreasing in $(0, d_1)$, an infinitesimal perturbation of mass from the origin would bring that mass into the free swarm, which is a more energetically favorable state.

Nevertheless, $\bar{\rho}$ are steady states and, as demonstrated in section 3.3.1, are asymptotically stable with respect to *certain* perturbations; given the considerations above, it is clear that such perturbations must only be with respect to the aggregation in the free swarm. Also shown in section 3.3.2, the dynamic evolution of model (2) consistently achieves (asymptotically) disconnected steady states starting from a diverse set of initial densities, which make such equilibria very relevant for the dynamics. Figure 1(a) shows in fact the disconnected equilibrium (26) achieved via particle simulations: Stars represent particles, and the cross indicates a superposition of particles at the origin.

(ii) *Connected equilibria.* There are two possible connected equilibria. The first is a degenerate case of (26), where $d_1 = d_2 = 0$ and all mass lies at the origin (or by translation, at any point in $(0, \infty)$):

$$\bar{\rho}(x) = M\delta(x). \tag{35}$$

While (35) is an equilibrium solution, it is not an energy minimizer, as can be inferred from the expression of Λ,

$$\Lambda(x) = -\frac{1}{2}M|x| + \frac{1}{2}Mx^2,$$

by noting that (14) is not satisfied for $x \in (0, 1)$. Any perturbation from this trivial equilibrium that takes an infinitesimal amount of mass from the delta concentration and puts it in the interior of Ω would result either in a disconnected state or in the connected equilibrium discussed below.

The other connected equilibrium can be obtained as a limiting case $d_1 \to 0$ of the disconnected equilibria (26) (see also (31)). In this limit, there is no delta aggregation on the wall ($S = 0$), $d_2 = 1$, and the solution consists in a constant density in the interval $(0, 1)$; see the solid line in Figure 1(b). Alternatively, one can consider an entire family of such solutions by taking arbitrary translations of the constant swarm to the right; this in fact corresponds to the equilibrium solution in the absence of boundaries, as discussed in section 2. The connected state is a swarm minimizer, as can be inferred by a direct calculation of $\Lambda(x)$; for an illustration, see the dashed line in Figure 1(b).

The energy corresponding to the equilibria (26) can be easily computed from (5), (11), and (28) by noting that in the absence of an external potential,

$$E[\bar{\rho}] = \frac{1}{2}\int_{\Omega_{\bar{\rho}}} \Lambda(x)\bar{\rho}(x)dx = \frac{\lambda_1}{2}\int_{\Omega_1} \bar{\rho}(x)dx + \frac{\lambda_2}{2}\int_{\Omega_2} \bar{\rho}(x)dx.$$

After a simple calculation, using the explicit expressions of λ_1 and λ_2 from (32), one finds

$$E[\bar{\rho}] = \frac{M^2}{3}\left(d_1^3 - \frac{1}{8}\right) = \frac{M^2}{24}d_2(-3 + 3d_2 - d_2^2). \tag{36}$$

Note that $E[\bar{\rho}]$ has the lowest energy for $d_1 = 0$ (or, equivalently, $d_2 = 1$), which corresponds to the (limiting) connected equilibrium.

Remark 3.1. The equilibria discussed above can be alternatively parametrized by r_M, defined as the mass ratio between the mass in the free swarm and the mass accumulated at the boundary of the domain (the origin in this case). This is in fact the parametrization used for the two-dimensional study in section 4 (see (74)). In one dimension, the mass ratio of the two components (cf. (26) and (31)) is given by

$$r_M = \frac{Md_2}{S} = \frac{d_2}{1-d_2}.$$

The parameter d_2 ranges in $(0,1)$ for the disconnected equilibria in part (i), while the connected equilibria in part (ii) correspond to $d_2 = 0$ and $d_2 = 1$, respectively. Consequently, in the absence of an exogenous potential, an equilibrium exists for any $r_M \in [0,\infty)$, as well as $r_M = \infty$. However, the only equilibrium that is an energy minimizer, and hence stable, is the one with infinite mass ratio, corresponding to the connected steady state which has all mass in the free swarm; see Figure 1(b).

Figure 1(c) shows a plot of the energy $E[\bar{\rho}]$ calculated in (36) as a function of mass ratio r_M. We find a monotonically decreasing profile with the lowest energy state corresponding to the connected equilibrium with all mass in the free swarm ($r_M = \infty$). The connected equilibrium ($d_2 = 1$ and $d_1 = 0$) is in fact the global minimizer in this case, as one can infer from the remark below.

Remark 3.2. To conclude that the connected equilibrium is the global minimizer, one needs to consider other possible minimizers and show that their energies are larger. We have already shown that disconnected equilibria of form (26) are not minimizers. One can also show that a multicomponent free swarm is not an energy minimizer either. Following [7], we wish to show that $\Lambda(x)$ is convex between free swarm components, which is a sufficient condition to show that it is not an energy minimizer as (17) does not hold.

Assume a disconnected equilibrium of the form

$$\rho(x) = S\delta(x) + \sum_{i=1}^{m} \rho_i(x), \tag{37}$$

where ρ_i are supported on Ω_i (Ω_i are disjoint from each other and do not include the origin). Note that by (24), $\rho_i(x) = M$ for $x \in \Omega_i$, though this is not directly used below to show that equilibrium (37) is not a minimizer.

Then (11) becomes

$$\Lambda(x) = S\left(\frac{1}{2}x^2 - \frac{1}{2}x\right) + \sum_{i=1}^{m} \int_{\Omega_i} K(x-y)\rho_i(y)\,\mathrm{d}y,$$

and for $x \notin \cup\Omega_i$ one gets

$$\Lambda''(x) = S + \sum_{i=1}^{m} \int_{\Omega_i} \rho_i(y)\,\mathrm{d}y = M > 0.$$

Therefore, $\Lambda(x)$ is indeed convex between free swarm components, and (37) cannot be a minimizer.

3.2. Linear exogenous potential. Consider the exogenous gravitational potential $V(x) = gx$, with $g > 0$. The domain of the problem is, again, the half-line $\Omega = [0, \infty)$. As $V''(x) = 0$, we infer from (25) that an equilibrium has constant density M in the part of its support which is not on the boundary.

We focus, as in section 3.1, on equilibria that have possibly disconnected components and look for steady states in the form (26), consisting of a delta aggregation at the origin and a constant density M in the interval $(d_1, d_1 + d_2)$, where $d_1 \geq 0$, $d_2 > 0$. As above, the support $\Omega_{\bar{\rho}}$ consists of two components, $\Omega_1 = \{0\}$ and $\Omega_2 = [d_1, d_1 + d_2]$, and the constant mass condition yields (27).

Equilibria (26) must satisfy the necessary condition (16), which in this case reduces to (28). By direct calculation,

$$\Lambda(x) = S\left(\frac{1}{2}x^2 - \frac{1}{2}x\right) + \int_{d_1}^{d_1+d_2}\left(\frac{1}{2}(x-y)^2 - \frac{1}{2}|x-y|\right)M\,dy + gx. \tag{38}$$

By evaluating at $x \in (d_1, d_2)$ and requiring that $\Lambda(x)$ be constant in this interval, we arrive at the following constraints on the parameters. First, by setting to zero the coefficient of x^2, we find (27), which represents the mass constraint condition. Then we note that the coefficient of x vanishes, provided that

$$S = M(2d_1 + d_2)(1 - d_2) + 2g.$$

Combine this equation with the mass constraint (27) to find

$$S = M(1 - d_2), \qquad d_1 = -\frac{g}{M(1-d_2)} + \frac{1-d_2}{2}. \tag{39}$$

Note that since $d_1 \geq 0$ and $0 < d_2 < 1$, then necessarily $g < \frac{M}{2}$ and $0 < d_2 \leq 1 - \sqrt{\frac{2g}{M}}$.

Denote by $g_c = \frac{M}{2}$ this critical value of g. From the above we conclude that for any $g < g_c$, we have a family of solutions to (16) of the form (26) with parameter $d_2 \in (0, 1 - \sqrt{\frac{2g}{M}}]$. For any d_2 in the open interval $(0, 1 - \sqrt{\frac{2g}{M}})$, $d_1 > 0$, and hence these states are disconnected. For $d_2 = 1 - \sqrt{\frac{2g}{M}}$, $d_1 = 0$ and the state is connected. Also, from (39), we infer that the center of mass $d_1 + \frac{d_2}{2}$ of the free swarm is located at $\frac{1}{2} - \frac{g}{S}$.

For $g > g_c$ there are no equilibria in the form (26). As shown below, the equilibrium in this case is a delta accumulation at the origin, which is also a global minimizer of the energy. Physically this can be explained by having a threshold value g_c beyond which the gravity is so strong that it pins all mass on the boundary.

We consider now the two cases $g < g_c$ and $g > g_c$.

Case $g < g_c$. As noted above (cf. (39)), there exists a family of solutions to (16) of the form (26), parametrized by $d_2 \in (0, 1 - \sqrt{\frac{2g}{M}}]$. By an elementary calculation, one can compute

the values of $\Lambda(x)$ in each component of the support, Ω_1 and Ω_2, respectively:

$$\lambda_1 = -\frac{M}{24}(1-d_2)^3 + \frac{M}{8}(1-d_2)^2 - \frac{M}{12} + \frac{g^2}{2M}\frac{d_2}{(1-d_2)^2}, \tag{40a}$$

$$\lambda_2 = -\frac{M}{24}(1-d_2)^3 - \frac{M}{12} - \frac{g^2}{2M}\frac{1}{1-d_2} + \frac{g}{2}. \tag{40b}$$

As in the zero gravity case, we find that $\lambda_1 > \lambda_2$ unless $d_2 = 1 - \sqrt{\frac{2g}{M}}$ (or, equivalently, $d_1 = 0$), in which case $\lambda_1 = \lambda_2$. We discuss separately the disconnected and connected states.

(i) *Disconnected equilibria ($d_1 > 0$, $d_2 < 1-\sqrt{\frac{2g}{M}}$).* A generic disconnected solution to (28) (here $g = 0.125$) is shown in Figure 2(a); the solid line indicates the constant density in the free swarm, and the circle on the vertical axis indicates the strength of the delta aggregation. To show that these states are equilibria, one need only check the velocity in Ω_1, the boundary of the domain. By an argument similar to that in the zero gravity case (attractive and repulsive effects at the origin are only felt through interactions with the free swarm), the velocity $v(0)$ calculated from (2b) reads as

$$v(0) = P_0\left(-\int_{\Omega_2} K'(-y)\bar{\rho}(y)dy - g\right). \tag{41}$$

By (34) and (39),

$$-\int_{\Omega_2} K'(-y)\bar{\rho}(y)dy = -g\frac{d_2}{1-d_2},$$

and hence, from (41) and (3) we find that

$$v(0) = P_0\big(\underbrace{-\frac{g}{1-d_2}}_{<0}\big) = 0.$$

The disconnected state is indeed an equilibrium.

By a direct calculation, one can find from (38) and (39)

$$\Lambda'(x) = M(x-d_1) \quad \text{for } x \in (0,d_1) \quad \text{and} \quad \Lambda'(x) = M(x-d_1-d_2) \quad \text{for } x \in (d_1+d_2,\infty),$$

and hence, $\Lambda(x)$ is strictly decreasing in $(0,d_1)$ and strictly increasing in (d_1+d_2,∞); see the dashed line in Figure 2(a). We infer that disconnected equilibria $\bar{\rho}$ in the form (26) are *not* local minima; again, (14) is not satisfied near the origin, and an infinitesimal perturbation of mass from Ω_1 (boundary) would bring it into Ω_2 (free swarm). Nevertheless, these equilibria are asymptotically stable to certain perturbations of the free swarm, and our numerical explorations indicate, as in the zero gravity case, that such disconnected steady states are very relevant for model (2), as they are reached dynamically starting from a wide range of initial densities; see sections 3.3.1 and 3.3.2. Figure 2(a) shows this particular disconnected equilibrium obtained via particle simulations (stars and cross).

(ii) *Connected equilibria.* There are two different connected equilibria: one that has all mass at the origin, and another that corresponds to the limit case $d_1 = 0$, $d_2 = 1 - \sqrt{\frac{2g}{M}}$ of the disconnected equilibria in part (i) above.

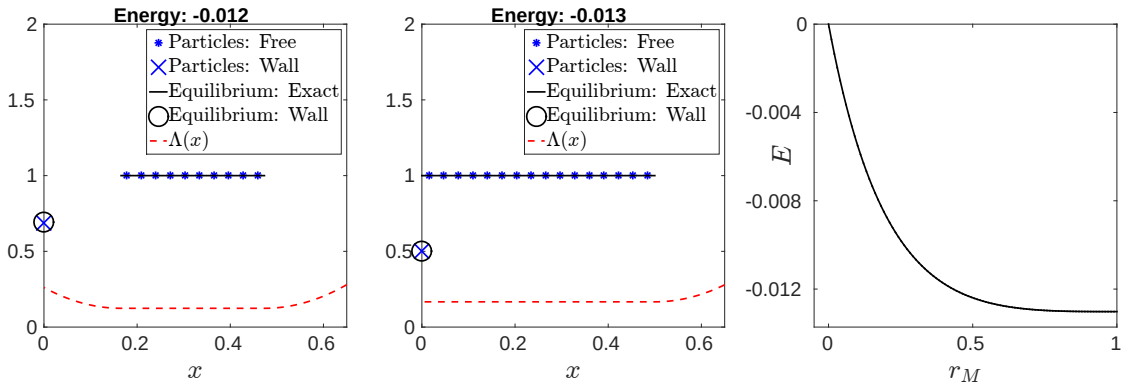

(a) (b) (c)

Figure 2. *Equilibria* (26) *on half-line for* $V(x) = gx$ *(linear exogenous potential) with* $g = 0.125$. (a) *Disconnected state consisting in a free swarm of constant density and a delta aggregation at the origin.* (b) *Connected state with a constant density in a segment adjacent to the origin and a delta aggregation at the origin.* (c) *Energy of equilibria* (26) *as a function of the mass ratio; the lowest energy state corresponds to the connected equilibrium* ($r_M = \sqrt{\frac{M}{2g}} - 1$).

The first type is a delta concentration at the origin of strength M, as in (35). This can be thought of as a degenerate case of (26) with $d_1 = d_2 = 0$. The calculation of Λ from (11) yields

$$\Lambda(x) = -\frac{1}{2}M|x| + \frac{1}{2}Mx^2 + gx.$$

Since $\Omega_{\bar{\rho}} = \{0\}$, (13) trivially holds with $\lambda = 0$, while (14) is equivalent to

$$\left(-\frac{1}{2}M + \frac{1}{2}Mx + g\right)x > 0 \qquad \text{for all } x > 0. \tag{42}$$

The inequality above does not hold when $g < \frac{M}{2}$; hence the equilibrium (35) is not an energy minimizer when $g < g_c$.

The other type of connected equilibrium is obtained from the disconnected equilibria in part (i) in the limit $d_1 \to 0$; it consists of a delta aggregation at the origin of strength $S = \sqrt{2gM}$ and a constant density M in the interval $(0, 1 - \sqrt{\frac{2g}{M}})$. The connected equilibrium for $g = 0.125$ and $M = 1$ is illustrated in Figure 2(b); see the solid line and circle on the vertical axis indicating the strength of the delta aggregation. The connected state is a swarm minimizer, as can be inferred from a direct calculation of $\Lambda(x)$; see the dashed line in Figure 2(b).

The energy corresponding to the equilibria (26) in the gravity case can be computed through elementary calculations from (5), (11), and (16), along with the expressions of λ_1 and λ_2 from (40). We omit the details and list only the final outcome:

$$E[\bar{\rho}] = \frac{M^2}{24}d_2(-3 + 3d_2 - d_2^2) + \frac{g}{2}Md_2 - \frac{g^2}{2}\frac{d_2}{1 - d_2}. \tag{43}$$

The zero gravity calculation (36) can be obtained from (43) by setting g to zero. Also as expected, from (43) we find that the energy is decreasing with respect to d_2:

$$\frac{\partial E}{\partial d_2} = -\frac{1}{2}\left(\frac{M}{2}(d_2-1) - g\frac{1}{d_2-1}\right)^2 \leq 0.$$

Hence, among all equilibria in the form (26), the one that has the lowest energy is the connected state, corresponding to $d_2 = 1 - \sqrt{\frac{2g}{M}}$.

Remark 3.3. As noted in Remark 3.1, the family of equilibria above can be alternatively parametrized by r_M, the mass ratio between the mass in the free swarm and the mass on the wall. By (39), r_M is given by

$$r_M = \frac{Md_2}{S} = \frac{d_2}{1-d_2}. \tag{44}$$

The parameter d_2 ranges in $(0, 1-\sqrt{\frac{2g}{M}})$ for the disconnected equilibria, while $d_2 = 0$ and $d_2 = 1 - \sqrt{\frac{2g}{M}}$ correspond to the two connected equilibria discussed above. Hence, $r_M \in [0, \sqrt{\frac{M}{2g}} - 1]$ or, equivalently, $r_M \in [0, \sqrt{\frac{g_c}{g}} - 1]$.

Figure 2(c) shows the energy (43) of the equilibria in the form (26) for the gravitational potential with $g = 0.125$, plotted as a function of the mass ratio r_M. Note the monotonically decreasing profile, with the equilibrium of lowest energy being the connected state shown in Figure 2(b); this equilibrium corresponds to the largest possible value of mass ratio, which in this case is $r_M = 1$. By an argument similar to that in Remark 3.2, one can in fact infer that the connected equilibrium is a global minimizer.

A schematic of the existence and stability of equilibria in one dimension is shown in Figure 3(a). Note that the only stable equilibrium for $g < g_c$ is the connected state with $r_M = \sqrt{\frac{g_c}{g}} - 1$. Also, the closer the gravity to the critical value g_c, the smaller the range of possible mass ratios; at critical value $g = g_c$ the interval collapses to $r_M = 0$ (no free swarm). On the other hand, in the limit of vanishing gravity $g \to 0$, an equilibrium exists for any mass ratio $r_M \in [0, \infty)$ (including infinite mass ratio), as is consistent with the zero gravity case studied in section 3.1; see also Remark 3.1.

Case $g > g_c$. The equilibrium solution in this case consists in a delta concentration at the origin (see (35)). As noted above, for such equilibrium, (14) is equivalent to (42), which holds trivially when $g \geq \frac{M}{2}$. We conclude from here that (35) is an energy minimizer. This fact is also illustrated in the schematic from Figure 3(a): The only (stable) equilibrium when $g > g_c$ is the configuration with all mass at the origin ($r_M = 0$), which is in fact a global minimizer.

3.3. Dynamic evolution of the aggregation model.

In this section we investigate the dynamics of model (2), with a focus on how and how often the equilibria (26) are reached dynamically. In particular, we determine under which perturbations the equilibria (26) are asymptotically stable.

3.3.1. Reduced dynamics and basins of attraction.

In this study of the dynamics we assume a fixed amount of mass S on the wall and an arbitrary density profile ρ_2 in the interior of Ω. We wish to quantify the dynamics of the support of ρ_2 and its center of mass. We achieve

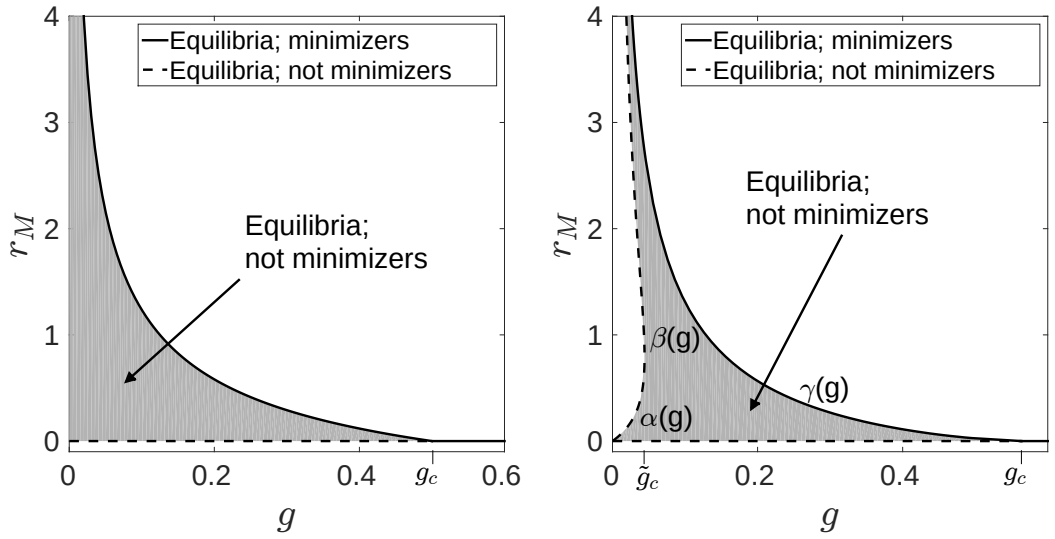

Figure 3. *Existence and stability of connected and disconnected equilibria. Highlighted in gray are regions where equilibria exist but are not minimizers.* (a) *One dimension,* $V(x) = gx$, $g_c = 0.5$. *For* $0 < g < g_c$, *disconnected equilibria in the form* (26) *exist for all mass ratios* $r_M \in (0, \sqrt{\frac{g_c}{g}} - 1)$; *these equilibria are not energy minimizers. The only stable equilibrium is the connected state with* $r_M = \sqrt{\frac{g_c}{g}} - 1$ *(solid line). For* $g > g_c$, *there exists no equilibrium in the form* (26). *The trivial equilibrium where all mass lies at the origin* ($r_M = 0$) *is unstable for* $g < g_c$ *(dashed line), but it is a global minimizer when* $g > g_c$ *(solid line).* (b) *Two dimensions,* $V(x_1, x_2) = gx_1$, $\tilde{g}_c \approx 0.044$, $g_c \approx 0.564$. *For* $0 < g < \tilde{g}_c$, *disconnected equilibria in the form* (66) *exist only for mass ratios* $r_M \in (0, \alpha(g)) \cup (\beta(g), \gamma(g))$, *while for* $\tilde{g}_c < g < g_c$, *disconnected equilibria exist for* all *mass ratios* $r_M \in (0, \gamma(g))$; *none of these disconnected equilibria are energy minimizers. The only stable equilibrium for* $0 < g < g_c$ *is the connected state with* $r_M = \gamma(g)$ *(solid line). For* $g > g_c$, *there exists no equilibrium in the form* (66). *The equilibrium* (75) *that has all mass on the wall* ($r_M = 0$) *is unstable for* $g < g_c$ *(dashed line), but it is a global minimizer when* $g > g_c$ *(solid line).*

explicit expressions defining the support of ρ_2 and its center of mass which will hold up until mass is transferred onto or off of the wall. Furthermore, we derive conditions for this transfer to happen and thus identify when the assumption of having a fixed amount of mass on the wall is violated.

Consider the evolution in (2) of a time-dependent density that has two distinct components:

$$\rho(x,t) = \rho_1(x) + \rho_2(x,t), \tag{45}$$

where $\rho_1(x) = S\delta(x)$ is a delta aggregation at the origin (with S fixed) and $\rho_2(x,t)$ is the density profile of the free swarm, with support $\Omega_2(t) = [a(t), b(t)]$. Here, $b(t) > a(t) > 0$ holds up until the time when the free swarm touches the wall.

Let

$$M_2 = \int_{\Omega_2(t)} \rho_2(x,t)\,\mathrm{d}x \quad \text{and} \quad C_2(t) = \frac{\int_{\Omega_2(t)} x\rho_2(x,t)\,\mathrm{d}x}{M_2} \tag{46}$$

be the mass and the center of mass of the free swarm, respectively. Note that since the mass on the wall is fixed, M_2 does not depend on t and we have $M_2 = M - S$.

Solutions of form (45) satisfy (2) in the weak sense. Note that (2) is an equation in conservation law form, and its weak formulation is standard [24]. Assume that in the free swarm the solution $\rho_2(x,t)$ is smooth enough so that (2) holds in the classical sense. By a standard argument [24, Chapter 3.4] one can then derive the Rankine–Hugoniot conditions which give the evolution of the two discontinuities $a(t)$ and $b(t)$. For instance, the evolution of the left end is given by

$$\frac{\mathrm{d}a}{\mathrm{d}t} = v(a,t), \tag{47}$$

and by (2b), (18), and (19) we calculate

$$\begin{aligned} v(a,t) &= -aS + \frac{S}{2} - \int_{\Omega_2} \left(a - y + \frac{1}{2}\right) \rho_2(y,t)dy - g \\ &= -Ma + M_2 \left(C_2 - \frac{1}{2}\right) + \frac{S}{2} - g. \end{aligned}$$

By a similar calculation,

$$\begin{aligned} \frac{\mathrm{d}b}{\mathrm{d}t} &= v(b,t) \\ &= -Mb + M_2 \left(C_2 + \frac{1}{2}\right) + \frac{S}{2} - g. \end{aligned}$$

Finally, we derive the evolution of the center of mass of ρ_2 and close the system. Multiply (2a) by x, integrate over Ω_2, and use integration by parts in the right-hand side to get

$$\int_{\Omega_2(t)} x(\rho_2)_t \,\mathrm{d}x = (x\rho_2(K*\rho_1 + K*\rho_2 + V)_x)\Big|_a^b - \int_{\Omega_2} \rho_2(K*\rho_1 + K*\rho_2 + V)_x \,\mathrm{d}x. \tag{48}$$

By an elementary calculation,

$$\frac{\mathrm{d}}{\mathrm{d}t}\int_{\Omega_2(t)} x\rho_2(x,t)\,\mathrm{d}x = \int_a^b x(\rho_2)_t \,\mathrm{d}x + \rho_2(b,t)b\frac{\mathrm{d}b}{\mathrm{d}t} - \rho_2(a,t)a\frac{\mathrm{d}a}{\mathrm{d}t}. \tag{49}$$

Combine (48) and (49), and use the evolution of $a(t)$ and $b(t)$ derived above. The boundary terms cancel, and we find

$$M_2\frac{\mathrm{d}C_2}{\mathrm{d}t} = -\int_{\Omega_2} \rho_2(K*\rho_1 + K*\rho_2 + V)_x \,\mathrm{d}x. \tag{50}$$

By symmetry of K,

$$\int_{\Omega_2} \rho_2(K*\rho_2)_x \,\mathrm{d}x = 0,$$

and with (18) and $V(x) = gx$ we get

$$(K * \rho_1)_x = S\left(x - \frac{1}{2}\right), \quad V_x = g,$$
$$\int_{\Omega_2} \rho_2 (K * \rho_1 + V)_x \, \mathrm{d}x = SM_2C_2 + M_2\left(g - \frac{S}{2}\right).$$

Hence, from (50) one can derive the evolution of C_2, which together with the evolution of a and b yields the following system of evolution equations:

$$\frac{\mathrm{d}C_2}{\mathrm{d}t} = -SC_2 + \left(\frac{S}{2} - g\right), \tag{51a}$$
$$\frac{\mathrm{d}a}{\mathrm{d}t} = -Ma + M_2\left(C_2 - \frac{1}{2}\right) + \frac{S}{2} - g, \tag{51b}$$
$$\frac{\mathrm{d}b}{\mathrm{d}t} = -Mb + M_2\left(C_2 + \frac{1}{2}\right) + \frac{S}{2} - g. \tag{51c}$$

It is now an elementary exercise to solve (51) for $C_2(t)$, $a(t)$, and $b(t)$ given initial data $C_2(0), a(0)$, and $b(0)$. One then gets

$$C_2(t) = \left(C_2(0) - \frac{1}{2} + \frac{g}{S}\right)e^{-St} + \left(\frac{1}{2} - \frac{g}{S}\right), \tag{52a}$$
$$a(t) = \left(C_2(0) - \frac{1}{2} + \frac{g}{S}\right)e^{-St} + \left(a(0) - C_2(0) + \frac{M_2}{2M}\right)e^{-Mt} + \left(\frac{S}{2M} - \frac{g}{S}\right), \tag{52b}$$
$$b(t) = \left(C_2(0) - \frac{1}{2} + \frac{g}{S}\right)e^{-St} + \left(b(0) - C_2(0) - \frac{M_2}{2M}\right)e^{-Mt} + \frac{1}{2MS}\left(M^2 - 2Mg - M_2^2\right). \tag{52c}$$

An initial observation is that provided our assumptions hold for all $t \geq 0$ (i.e., the mass on the wall is fixed and $a(t) > 0$), the equilibrium solution for (51) corresponds to the disconnected state (26). Indeed, one can check that at the equilibrium for (51), $a = d_1$, $b = d_1 + d_2$, and $C_2 = d_1 + \frac{d_2}{2}$, with d_1 and d_2 given by (39) in terms of S. We also mention that we are discussing only realistic cases ($C_2(0) \geq 0$, $a(0) \geq 0$). Some arguments made below would not be true if we considered unrealistic cases, but, of course, these exceptions are irrelevant.

Next we wish to use the reduced dynamics to determine under which perturbations the disconnected equilibria (26) are asymptotically stable. By inspecting the profile of $\Lambda(x)$, we have already observed that these equilibria are unstable under infinitesimal perturbations which move mass off the wall (see Figures 1 and 2). Therefore disconnected equilibria can only be (asymptotically) stable with respect to perturbations of the free swarm. We take such a perturbation and consider the evolution of a density of the form

$$\rho(x,t) = \bar{\rho}(x) + \tilde{\rho}_2(x,t), \tag{53}$$

where $\bar{\rho}$ is the disconnected equilibrium (26) and $\tilde{\rho}_2$ has support away from the origin and zero mass. Note that density (53) can also be written in the separated form (45), where

$$\rho_1(x) = S\delta(x) \qquad \text{and} \qquad \rho_2(x,t) = M\mathbb{1}_{(d_1, d_1+d_2)}(x) + \tilde{\rho}_2(x,t) \tag{54}$$

such that $\rho(x,t) = \rho_1(x) + \rho_2(x,t)$.

The reduced dynamics (51) can be used to track the dynamics of the center of mass $C_2(t)$ and the support $[a(t), b(t)]$ of $\rho_2(x,t)$, provided that

(i) no mass leaves the origin, *and*

(ii) no mass transfers from ρ_2 to the origin.

We will now quantify when (i) and (ii) can happen. To address (i), one needs to inspect the velocity at the origin, which, computed by (2b) and (18) (see also (46)), gives

$$\begin{aligned} v(0,t) &= P_0 \left(\int_{\Omega_2(t)} \left(y - \frac{1}{2} \right) \rho_2(y,t)\, \mathrm{d}y - g \right) \\ &= P_0 \left(M_2 \left(C_2(t) - \frac{1}{2} \right) - g \right). \end{aligned}$$

We find that no mass leaves the origin ($v(0,t) = 0$), provided that

$$C_2(t) \leq \frac{1}{2} + \frac{g}{M_2}. \tag{55}$$

In particular, the initial perturbed state $\rho(\cdot, 0)$ in (53) must satisfy this restriction at $t = 0$. We note that once (55) holds at $t = 0$, it holds for all times; this can be inferred from the monotonic evolution of $C_2(t)$ (see (52a)), where

$$\lim_{t\to\infty} C_2(t) = \frac{1}{2} - \frac{g}{S} < \frac{1}{2} + \frac{g}{M_2}.$$

For (ii), we note that mass transfer occurs when the left end of the support of the free swarm meets the wall and pushes into it. Mathematically, this amounts to having $a = 0$ and $\frac{\mathrm{d}a}{\mathrm{d}t} < 0$ hold simultaneously. Alternatively, we can simply find any cases where $a(t) < 0$ at some time. Using the explicit solutions (52), we find exactly the region of $(a(0), C_2(0))$ which yields $a(t) < 0$ for $t > 0$ and $C_2(t) > 0$. Denote the boundary $a(t) = 0$ for $t > 0$ and $C_2(t) > 0$ by γ_0, such that any points $(a(0), C_2(0))$ below γ_0 correspond to points where the evolution would have mass from ρ_2 transferring to the origin. Figure 4 illustrates the curves γ_0 (solid lines) for various mass ratios r_M (or, equivalently, for various delta strengths S). Initial conditions $(a(0), C_2(0))$ above γ_0 correspond to points where evolution would not transfer mass from ρ_2 to the origin and (51) holds for all time as long as $C_2(0) \leq \frac{1}{2} + \frac{g}{M_2}$; also note that, necessarily, $C_2(0) > a(0)$.

In summary, one takes an initial perturbed state $\rho(\cdot, 0)$ in (53) and considers the center of mass, $C_2(0)$, and the left edge of its support, $a(0)$. As long as no mass leaves the origin and no mass transfers from the free swarm to the wall, then (51) holds. Moreover, since we consider only perturbations that have zero mass and do not perturb the mass on the wall, then M_2 and S of the perturbed state will be the same as for the disconnected equilibrium $\bar{\rho}(x)$. By uniqueness of the solution (see (51)), we then know that

$$\lim_{t\to\infty} \rho(x,t) = \bar{\rho}(x).$$

Therefore perturbations for which the perturbed state satisfies $C_2(0) \leq \frac{1}{2} + \frac{g}{M_2}$ (condition (i)) and $(a(0), C_2(0))$ is above γ_0 (condition (ii)) are exactly the perturbations to which the disconnected equilibrium $\bar{\rho}(x)$ is asymptotically stable. Certain remarks are in order.

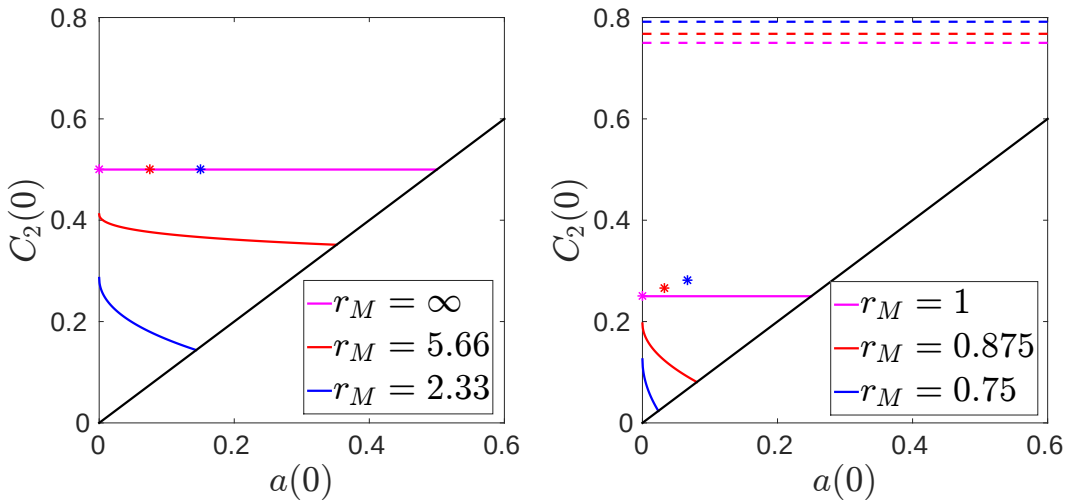

(a) (b)

Figure 4. *Disconnected equilibria (26) are asymptotically attracting certain initial densities of type (45). Considered are three mass ratios, one being the mass ratio of the minimizer (magenta) for $g = 0$ and $g = 0.125$. A perturbed state $\rho(x,t)$ (see (53) and (54)) that has $a(0)$ and $C_2(0)$ in the region strictly above the solid curves, representing γ_0, and below the dashed lines, $C_2(0) = 1/2 + g/M_2$, will evolve dynamically to the disconnected equilibrium of the corresponding mass ratio. An initial condition with $(a(0), C_2(0))$ below the solid curves will evolve dynamically to an equilibrium of a smaller mass ratio. The dashed lines indicate the thresholds $1/2 + g/M_2$ above which mass on the wall would lift off. Stars indicate the equilibrium for the mass ratio corresponding to its color, which gives a sense of how much the center of mass or the left edge of the support can be perturbed.*

Remark 3.4. The calculations above do not restrict the size of the perturbations $\tilde{\rho}$ in (53); the only restrictions are placed on the center of mass $C_2(0)$ and the left end point $a(0)$ of the perturbed free swarm at the initial time. Consequently, the basins of attraction of the disconnected equilibria are considerable in size and highly nontrivial. Section 3.3.2 will further elaborate on this point.

Remark 3.5. The connected equilibria ($r_M = \infty$ and $r_M = 1$) in Figure 4 and their corresponding magenta curves have been included only for illustration. Strictly speaking, we should have shown only mass ratios that correspond to disconnected equilibria for which the considerations in this subsection hold. Nevertheless, by a continuity argument, the magenta lines can be thought to correspond to disconnected equilibria that are arbitrarily close to the connected states. In fact, we infer from the figure that if we perturb the connected equilibrium such that the center of mass of the free swarm decreases (the centers of mass of the connected equilibria for $g = 0$ and $g = 0.125$ are at $1/2$ and $1/4$, respectively), then mass will transfer to the wall and result dynamically in a disconnected state.

Remark 3.6. Regarding the boundaries γ_0 shown in Figure 4, we found that there is a minimal mass ratio ($r_M \approx 1$ for $g = 0$ and $r_M \approx 0.6$ for $g = 0.125$) below which these curves do not cross through the relevant $0 < a(0) < C_2(0)$ region. For such mass ratios, any initial perturbation with $0 < a(0) < C_2(0) \leq 1/2 + g/M_2$ would dynamically result in (i) and (ii)

being satisfied for all times, and hence, equilibrium $\bar{\rho}$ being achieved at steady state. On the other hand, this observation also implies that equilibria $\bar{\rho}$ with mass ratios below this threshold cannot be achieved dynamically starting from initial densities with different mass ratios (as no mass transfer into the origin occurs below the threshold). This fact is also supported by the numerical simulations in section 3.3.2.

3.3.2. Nontrivial initial conditions leading to disconnected equilibria. We show in this section that a wide range of initial conditions can lead to disconnected states. Furthermore, we show that the mass ratios of the resultant states follow trends related primarily to the initial center of mass, and secondarily to how close the swarm is to the wall.

To this end we consider initial states of particles with positions randomly generated from a uniform distribution on $(d_1^{(i)}, d_1^{(i)} + d_2^{(j)})$, where $1 \le i, j \le 10$, and

$$d_1^{(i)} = \frac{1}{20}(i-1), \quad d_2^{(j)} = \frac{1}{10} j \quad \text{for} \quad g = 0, \tag{56}$$

$$d_1^{(i)} = \frac{1}{40}(i-1), \quad d_2^{(j)} = \frac{1}{20} j \quad \text{for} \quad g = 0.125. \tag{57}$$

We ran 50 particle simulations of $N = 1024$ particles for each interval $(d_1^{(i)}, d_1^{(i)} + d_2^{(j)})$, with $1 \le i \le 10$ and $1 \le j \le 10$. We evolved the particle simulations until the state is steady and calculated the mass ratio of the resultant state.

For convenience of discussion later, we denote the midpoint of the initial interval,

$$m_d = \frac{1}{2}\left(d_1^{(i)} + \left(d_1^{(i)} + d_2^{(j)}\right)\right). \tag{58}$$

We mention here as well that the center of mass of the initial swarm will be close to this midpoint, as we have drawn particle positions from a uniform distribution. This is particularly important in comparing with the results of section 3.3.1, as the intervals $(d_1^{(i)}, d_1^{(i)} + d_2^{(j)})$ have been constructed in such a way that for $i = 11 - j$ we have $m_d = \frac{1}{2}$ for $g = 0$ and $m_d = \frac{1}{4}$ for $g = 0.125$; see Figure 4 and Remark 3.5.

We find that for the $g = 0$ case, all initial states with $m_d < \frac{1}{2}$ resulted in a disconnected state, and all initial states with $m_d > \frac{1}{2}$ resulted in a connected state; see squares and circles in Figure 5(a) indicating percentages of disconnected states. This result is consistent with Remark 3.5. Furthermore, we see that for $m_d = \frac{1}{2}$ some resultant states were disconnected and some were connected, accounting for the fact that due to the random distribution of particles sometimes we have the center of mass larger than $\frac{1}{2}$ and sometimes smaller; see Figure 5(a).

For the case of $g = 0.125$ we find relatively similar results. Figure 5(b) shows that for $m_d < 0.15$ we always get disconnected resultant states, and for $m_d > 0.175$ we always get the connected equilibrium. For $m_d = 0.15$ and $m_d = 0.175$ the results can be mixed. We suspect in fact that there may be discrete numerical effects and that the true value of m_d where we observe variability in disconnected/connected resultant states is closer to $\frac{1}{4}$, consistent with Remark 3.5. A discrete effect that occurs for $g = 0$, for instance, is when the correct resultant state has mass on the wall which is greater than zero but less than that of two particles; this case cannot be identified by the particle method as disconnected. Also note that this error, which favors connected states, is more likely to occur for larger $d_1^{(i)}$.

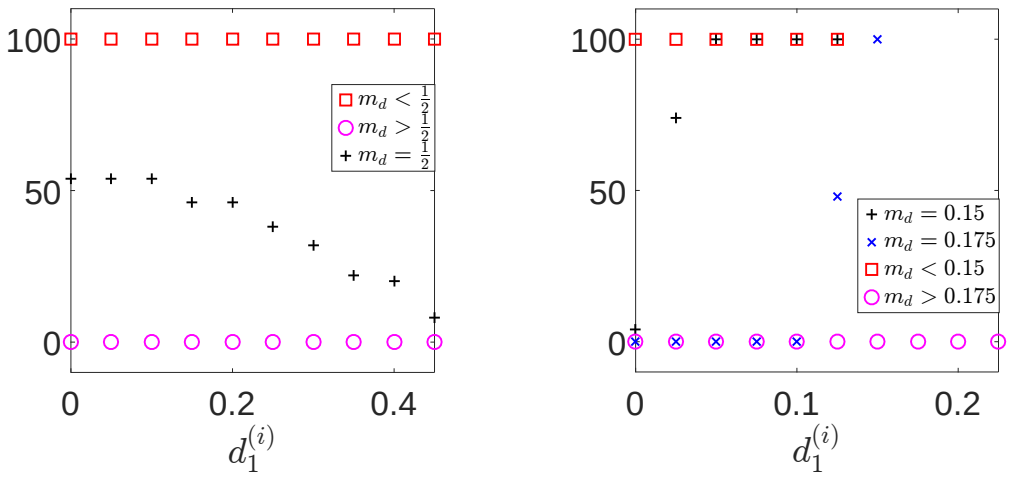

(a) (b)

Figure 5. *Percentage of initial states which resulted in disconnected states for* (a) $g = 0$ *and* (b) $g = 0.125$. *Note that we find disconnected resultant states for a significant set of initial data.*

We also computed the mass ratios of the resultant equilibria in these simulations and averaged over runs that have the same initial midpoint m_d. In both the gravity and no gravity cases we found that the average resultant mass ratio tends to be smaller for smaller m_d; see Figure 6. The results further support the fact that there indeed exists a minimal mass ratio for equilibria that can be achieved dynamically; see Remark 3.6.

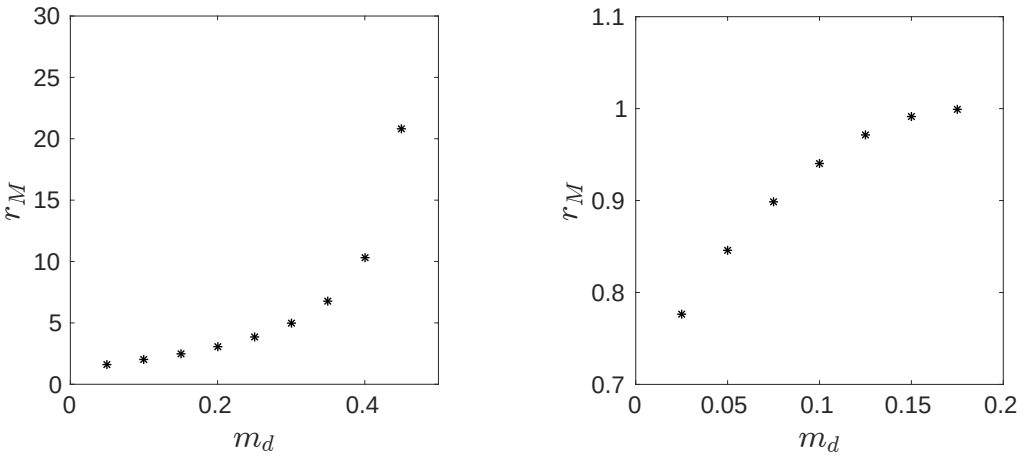

(a) (b)

Figure 6. *Average mass ratios of resultant states for particular* m_d *for* (a) $g = 0$ *and* (b) $g = 0.125$. $m_d = \frac{1}{2}$ *has been omitted from* (a) *for clarity, as the average is much larger (about* 516*).*

3.3.3. Discrete energy dissipation. We wish to demonstrate that particle simulations which lead to disconnected states obey a discrete-space, discrete-time analogue to (6). Let Δt be the length of time steps taken in a given particle simulation (see section 4.4.1 for details on the implementation of the particle method), and further, let $s = n\Delta t$ and $t = (n+1)\Delta t$ for $n \geq 0$ be two successive times in (6). We then have, after dividing by Δt,

$$\frac{E[(n+1)\Delta t] - E[n\Delta t]}{\Delta t} = -\frac{1}{\Delta t}\int_{n\Delta t}^{(n+1)\Delta t}\int_{\Omega} |P_x(-\nabla K * \rho(x,\tau) - \nabla V(x))|^2 \rho(x,\tau)\,\mathrm{d}x\,\mathrm{d}\tau. \tag{59}$$

We now check whether (59) holds in numerical simulations. For this purpose we pass to a discrete-space analogue as per a particle simulation with particles of equal weight, namely $\frac{M}{N}$, where N is the number of particles. Let x_i represent the position of particle i. The discrete density is a superposition of delta accumulations at the particle locations,

$$\rho^N(x,t) = \frac{M}{N}\sum_{i=1}^{N} \delta(x - x_i(t)),$$

and the corresponding discrete energy (see (5)) is given by

$$E[\rho^N] = \frac{M^2}{2N^2}\sum_{i=1}^{N}\sum_{j=1}^{N} K(x_i(t) - x_j(t)) + \frac{M}{N}\sum_{i=1}^{N} V(x_i(t)). \tag{60}$$

Note that $K(0) = 0$ in this context, so we do not need to exclude the case of $i = j$ in the double sum representing social interaction.

Figure 7 shows (solid lines) the left-hand side of (59) as computed from a particle simulation, with E given by (60). The simulations correspond to emerging disconnected equilibria. Shown there are $g = 0$ and $g = 0.125$. Also plotted in the figure (dashed lines), but indistinguishable at the scale of the figure, are discrete-time approximations of the right-hand side of (59); we used the trapezoidal rule to approximate the time integration and a discrete analogue of the projection operator P_x (cf. section 4.4.1). The difference between the two computed approximations falls within the discretization error of the particle method, and hence, the results show that the energy dissipation formula (59) holds at the discrete level. Note also that the energy decays for all times and levels off as it approaches the equilibrium.

3.4. Morse potential. In this subsection we consider the same problem setup as in section 3.1 except we use the Morse-type potential investigated in [7]:

$$K(x) = -GLe^{-|x|/L} + e^{-|x|}. \tag{61}$$

We consider the case of $G = 0.5$ and $L = 2$ throughout this subsection, as these values were one of the cases highlighted in [7]. The main point we want to make is that the findings above apply to the Morse potential as well. In particular, there is a one-parameter family of disconnected equilibria of model (2), which are not energy minimizers but are realized dynamically starting from a variety of initial conditions.

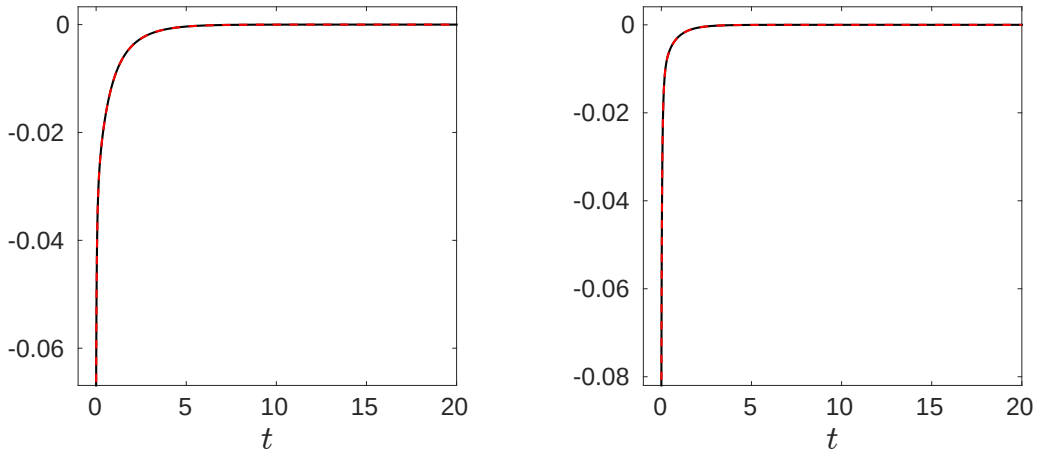

Figure 7. *Verification of the energy dissipation formula* (6) *for particle simulations where more than one particle joins the wall and disconnected states are emerging.* (a) $g = 0$, *and* (b) $g = 0.125$. *Approximations of the left-hand side of* (59) *(solid lines) and the right-hand side of* (59) *(dashed lines) fall within the discretization error. For the particular test shown here, the two approximations are within* 10^{-4} *(indistinguishable at the scale of the figure), which is consistent with the choice of* Δx *and* Δt.

One can find explicit forms for the equilibria for the Morse potential in just the same way as we found explicit forms for the potential (18)–(19). We assume the solution form

$$\bar{\rho}(x) = S\delta(x) + \rho_*(x)\mathbb{1}_{(d_1,d_1+d_2)}, \tag{62}$$

with

$$\rho_*(x) = C\cos(\mu x) + D\sin(\mu x) - \frac{\lambda_2}{\epsilon},$$
$$\mu = \sqrt{\frac{\epsilon}{\nu}}, \quad \epsilon = 2(GL^2 - 1), \quad \nu = 2L^2(1 - G). \tag{63}$$

The density ρ_* of the free swarm comes from the free space solution found in [7].

Then we seek to satisfy (cf. (28) and (8a))

$$\Lambda(0) = \lambda_1, \quad \Lambda(x) = \lambda_2 \quad \text{for } x \in [d_1, d_1 + d_2], \quad S + \int_{d_1}^{d_1+d_2} \rho_*(x)\,\mathrm{d}x = M. \tag{64}$$

The appendix shows the system of equations that arise from these conditions. We end up with four equations from requiring $\Lambda(x) = \lambda_2$ for $x \in [d_1, d_1 + d_2]$, as one can find that the constant term on the left-hand side is already λ_2 and the nonconstant terms comprise four linearly independent terms in x:

$$-GL\exp\left(-\frac{x}{L}\right), \quad \exp(-x), \quad -GL\exp\left(\frac{x}{L}\right), \quad \exp(x). \tag{65}$$

Together with $\Lambda(0) = \lambda_1$ and the mass constraint, this yields a system of six equations for seven unknowns (C, D, S, d_1, d_2, λ_1, and λ_2), indicating a one-parameter family of equilibria, as in sections 3.1 and 3.2. We solved numerically this system for various $S \in [0, 1]$ fixed.

Figure 8(a) shows a disconnected equilibrium found by solving (64); the circle indicates the delta strength at origin, and the solid line indicates the free swarm. The Λ profile (dashed line) shows that such disconnected equilibria are not energy minimizers (as in section 3.1). Figure 8(b) shows the connected equilibrium, which is in fact the free space solution from [7]. The connected equilibrium is an energy minimizer, as inferred from the Λ profile. In both plots note the excellent agreement with the particle simulations (crosses for delta aggregations and stars for free swarms). Finally, Figure 8(c) shows the energy of the equilibria (62) as a function of the mass ratio; as expected, the lowest energy is achieved by the connected state with $d_1 = 0$ (or, equivalently, $r_M = \infty$).

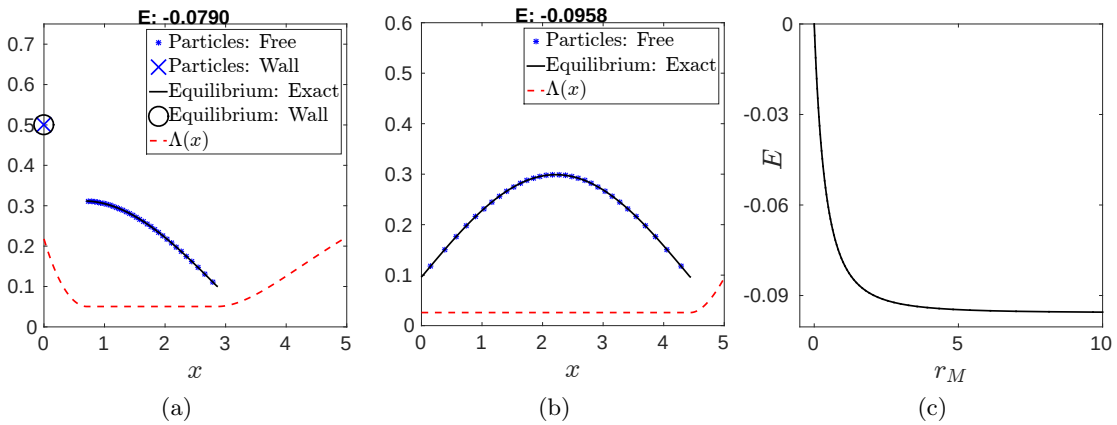

Figure 8. *Equilibria (62) on a half-line for $V(x) = 0$ (no exogenous potential). The interaction potential is given by (61), where $G = 0.5$ and $L = 2$. (a) Disconnected state. (b) Connected state with no aggregation at the origin; this is the same as the free space solution from [7]. (c) Energy of equilibria as a function of the mass ratio; the lowest energy state corresponds to the connected equilibrium $r_M = \infty$.*

The study in this subsection illustrates that the existence of (attracting) disconnected equilibria which are not minimizers and the existence of a minimizing equilibrium that is the connected state are not specific properties of the potential (18)–(19) but seem to be quite generic.

4. Two dimensions: Equilibria on a half-plane. We consider equilibria in two dimensions in the domain $\Omega = [0, \infty) \times \mathbb{R}$. The boundary $\partial\Omega = \{0\} \times \mathbb{R}$ can be interpreted as an impenetrable wall. The interaction kernel is given by (18)–(19), i.e., it consists of Newtonian repulsion and quadratic attraction.

4.1. No exogenous potential. As discussed in section 2, in the absence of boundaries the equilibrium is a constant density in a disk [27]; in two dimensions the value of this constant density is $2M$ (see (23)). Similar to the one-dimensional study, in domains with boundaries we expect to have equilibria that consist in swarms of constant densities *away* from the wall together with a possible aggregation buildup *on* the boundary.

Given the considerations above, we search for an equilibrium that consists of a constant density $2M$ in a bounded domain D that lies off the wall ($x_1 > 0$) and a Dirac delta accumulation on $\partial\Omega$. For consistency of notation with the study in one dimension, we take the horizontal extent of the free swarm D to be $d_1 < x_1 < d_1 + d_2$, with $d_1 \geq 0$, $d_2 > 0$. Also, we assume symmetry in the vertical direction and take the vertical extent of D to be given by the lower and upper free boundaries $x_2 = -g(x_1)$ and $x_2 = g(x_1)$, respectively.

Specifically,

$$D = \{(x_1, x_2) \mid d_1 < x_1 < d_1 + d_2, -g(x_1) < x_2 < g(x_1)\},$$

and the equilibrium we look for has the form

$$\bar{\rho}(x_1, x_2) = f(x_2)\delta_{\partial\Omega}(x_1, x_2) + 2M\, \mathbb{1}_D(x_1, x_2), \tag{66}$$

where the density profile $f(x_2)$ on the wall is assumed to have support $[-L, L]$.

The support $\Omega_{\bar{\rho}}$ of $\bar{\rho}$ consists of two components:

$$\Omega_1 = \{0\} \times [-L, L] \qquad \text{and} \qquad \Omega_2 = \bar{D}, \tag{67}$$

where the bar indicates the closure of the set.

As in one dimension, we focus our efforts on solving the necessary equilibrium condition (16). The unknowns in this case are the density profile f on the wall along with its extent L, and the free boundary g along with its horizontal extent given by d_1 and d_2. It can be immediately noted that this is a highly nonlinear problem, and, unlike in the one-dimensional case, a solution can only be sought numerically.

Denote the area of D by $|D|$. By the mass constraint (8a) we find

$$\int_{-L}^{L} f(x_2)dx_2 + 2M|D| = M. \tag{68}$$

Calculate $\Lambda(\mathbf{x})$ for $\mathbf{x} = (x_1, x_2) \in \Omega_{\bar{\rho}}$ using (11), where K is given by (18)–(19) and $V = 0$. A generic point $\mathbf{y} = (y_1, y_2) \in \Omega_{\bar{\rho}}$ can lie either on the wall or in D, along with its free boundary. Consequently, $\Lambda(\mathbf{x})$ consists of two terms:

$$\begin{aligned}\Lambda(\mathbf{x}) = &\int_{-L}^{L} \left(-\frac{1}{2\pi} \ln \sqrt{x_1^2 + (x_2 - y_2)^2} + \frac{1}{2}\left(x_1^2 + (x_2 - y_2)^2\right)\right) f(y_2)dy_2 \\ &+ 2M \iint_D \left(-\frac{1}{2\pi} \ln |\mathbf{x} - \mathbf{y}| + \frac{1}{2}|\mathbf{x} - \mathbf{y}|^2\right) \mathrm{d}\mathbf{y}.\end{aligned} \tag{69}$$

For an equilibrium, $\Lambda(\mathbf{x})$ has to be constant in each component of $\Omega_{\bar{\rho}}$:

$$\Lambda(\mathbf{x}) = \lambda_1 \quad \text{in } \{0\} \times [-L, L], \qquad \text{and} \qquad \Lambda(\mathbf{x}) = \lambda_2 \quad \text{in } \bar{D}. \tag{70}$$

Solving (70) numerically would be very expensive. First, it requires approximating Λ on a two-dimensional numerical grid, where at each grid point we would have to evaluate numerically a convolution integral. Second, it requires a nonlinear solver to solve (70) at all grid points of

this two-dimensional domain. We show below how one can reduce the dimensionality of the problem by making use of specific properties of the interaction potential.

Calculate the Laplacian of Λ from (69):

$$\begin{aligned}\Delta\Lambda(\mathbf{x}) &= 2\int_{-L}^{L} f(y_2)dy_2 + 2M\left(-1 + 2\iint_D \mathrm{d}\mathbf{y}\right)\\ &= 2\left(\int_{-L}^{L} f(y_2)dy_2 - M + 2M|D|\right),\end{aligned} \tag{71}$$

where for the first equality we used $\Delta(-\frac{1}{2\pi}\ln|\mathbf{x}|) = -\delta$; in particular, the logarithmic term in the single integral $\int_{-L}^{L}$ is harmonic for $\mathbf{x} \in D$.

Using the mass constraint (68), one can infer from (71) that Λ is harmonic in D:

$$\Delta\Lambda(\mathbf{x}) = 0 \qquad \text{for all } \mathbf{x} \in D. \tag{72}$$

This observation greatly simplifies the problem of solving (70). Indeed, provided that $\Lambda(\mathbf{x}) = \lambda_2$ is satisfied for $\mathbf{x} \in \partial D$ (i.e., only on the boundary of the free swarm), then by (72), using standard theory for harmonic functions, $\Lambda(\mathbf{x}) = \lambda_2$ for all $\mathbf{x} \in \bar{D}$. Consequently, (70) reduces to solving

$$\Lambda(\mathbf{x}) = \lambda_1 \quad \text{in } \{0\}\times[-L,L] \qquad \text{and} \qquad \Lambda(\mathbf{x}) = \lambda_2 \quad \text{on } \partial D. \tag{73}$$

We solve numerically (73) to find L, d_1, d_2, λ_1, λ_2, and the profiles f and g of the wall aggregation and the free boundary. Approximations for the latter are found on a uniform grid in the vertical, respectively, horizontal, direction. Details on the numerical implementation are presented in section 4.4.2; we only re-emphasize here that there is a huge computational gain in solving (73) versus (70) from having reduced the dimensionality of the problem.

As in the one-dimensional study, we find both disconnected and connected solutions to (73). We present them separately. We note again that in all numerical simulations presented in this paper, the mass M is set to 1.

Disconnected equilibria ($d_1 > 0$). As in one dimension, denote by r_M the ratio of the mass M_2 of the free swarm and the mass M_1 of the aggregation on wall:

$$r_M := \frac{M_2}{M_1} = \frac{2M|D|}{\int_{-L}^{L} f(x_2)dx_2}. \tag{74}$$

Numerical simulations suggest that disconnected solutions to (73) in the form (66) exist for all $r_M \in (0,\infty)$. In fact, based on numerical explorations, we believe that there is a unique disconnected solution to (73) for every $r_M \in (0,\infty)$ fixed. The limiting cases, i.e, the zero and infinite mass ratios, correspond to connected states, where all mass lies either *on* the wall or *off* the wall, respectively. These solutions will be elaborated below, where connected states are discussed.

To check whether the disconnected solutions are indeed equilibria, we compute numerically the velocity field at points on Ω_1, the part of the support that lies on the wall, and inspect its horizontal component (cf. Remark 2.2). For all the disconnected states we computed, we found

that velocity vectors at various points located near and at the edges of the wall aggregation point *toward* the interior of the domain Ω. Consequently, their projections are not zero (see (4)), and the states we computed are *not* equilibria. This result clearly shows that (16) is only a necessary, but not sufficient, condition for equilibrium; see Remark 2.2.

The conclusion reached above is exactly the opposite of what was found in one dimension, where all the disconnected solutions to (16) were steady states, though not local minima of the energy. The essentially different behavior is due to the two-dimensional geometry. In one dimension the distance from the wall to any point in the free swarm is necessarily parallel to the normal of the wall. In two dimensions this is not the case, and some interactions between the wall swarm and the free swarm can be farther than the distance from the wall to the furthest extent of the free swarm in the horizontal direction. This enables more attractive forces to come into play, most noticeably at the edges of the wall swarm $\mathbf{x} = (0, \pm L)$. Indeed, the edges of the wall swarm are where one finds the largest velocities normal to and pointing away from the wall, if one finds them at all.

Connected equilibria. The first type of connected equilibria corresponds to aggregations that lie entirely on the wall (no free swarm, $r_M = 0$). This is a degenerate case of densities of form (66), where D is the empty set. The equilibrium in this case has the form of a delta aggregation on the wall:

$$\bar{\rho}(x_1, x_2) = f(x_2)\delta_{\partial\Omega}(x_1, x_2). \tag{75}$$

We find the density profile $f(x_2)$ on the wall and its support $[-L, L]$ by solving numerically (13) in $\Omega_{\bar{\rho}} = \{0\} \times [-L, L]$. Note that the mass constraint (8a) implies

$$\int_{-L}^{L} f(x_2)dx_2 = M, \tag{76}$$

while in our case (13) reduces to

$$\int_{-L}^{L} \left(-\frac{1}{2\pi} \ln|x_2 - y_2| + \frac{1}{2}(x_2 - y_2)^2 \right) f(y_2)dy_2 = \lambda \qquad \text{for all } x_2 \in [-L, L]. \tag{77}$$

We solve numerically (76) and (77) to find f, L, and λ. The wall profile f is shown in Figure 9(a), along with the density profile obtained from particle simulations; note the excellent agreement between the two. We also note here that the only initial configurations that can dynamically evolve into this equilibrium are those with initial support on the wall.

With this numerically computed solution we then check (14), which here reads as

$$\int_{-L}^{L} \left(-\frac{1}{2\pi} \ln \sqrt{x_1^2 + (x_2 - y_2)^2} + \frac{1}{2}\left(x_1^2 + (x_2 - y_2)^2\right) \right) f(y_2)dy_2 \geq \lambda \qquad \text{for all } (x_1, x_2) \in \Omega_{\bar{\rho}}^c.$$

Note that $\Omega_{\bar{\rho}}^c$ is the disjoint union of the two semi-infinite vertical lines $\{0\} \times (-\infty, -L)$ and $\{0\} \times (L, \infty)$, with the open half-plane $(0, \infty) \times \mathbb{R}$. A colored contour plot of $\Lambda(x)$ is shown (on the right) in Figure 9(a). As expected, the inequality above does not hold near the wall, and hence, the equilibrium solution (75) is not an energy minimizer.

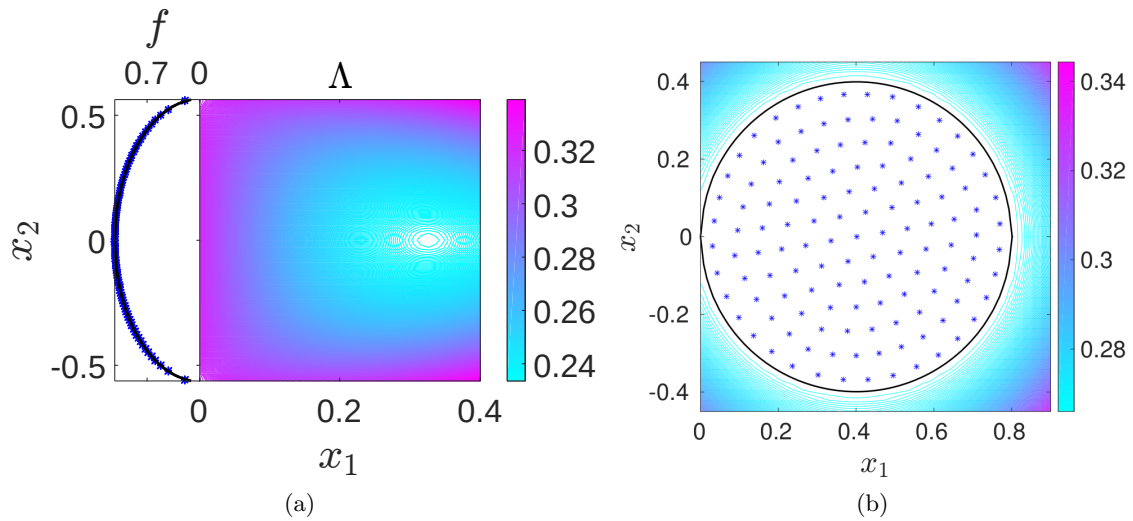

Figure 9. *Equilibria on a half-plane in two dimensions for $V = 0$ (no exogenous potential).* (a) *Equilibrium aggregation that lies entirely on the wall ($r_M = 0$). The solid line represents the density profile f on the wall as solved from (76) and (77). Note the excellent agreement with the particle simulations (blue stars). The equilibrium is not an energy minimizer, as indicated by the contour plot of Λ (shown at right).* (b) *Free swarm equilibrium ($r_M = \infty$) of constant density $2M$ in a disk of radius $\frac{1}{\sqrt{2\pi}}$. The contour plot of Λ, shown in the figure, demonstrates that this equilibrium is an energy minimizer. Note that there are no disconnected equilibria of form (66) in this case.*

We note in passing that integral equations with logarithmic kernels such as (77) arise in the representation of a harmonic function in terms of single-layer potentials. Various analytical and numerical results have been derived for such equations [39, 45]. These results do not apply to our setting, though, as in our problem the extent L of the boundary is also an unknown.

Connected equilibria of the second type correspond to swarm equilibria in free space and consist of a constant aggregation of density $2M$ in a disk of radius $\frac{1}{\sqrt{2\pi}}$. A representative equilibrium in this class can be considered the disk tangent to the wall at the origin; see Figure 9(b). This is an equilibrium in the form (66), where $f = 0$ (no delta aggregation on the wall) and $d_1 = 0$ (no separation). By taking arbitrary translations that keep the disk within Ω, one can then find a family of such constant aggregations. The constant density equilibria are swarm minimizers, as (14) can be shown to hold; a contour plot of Λ is also illustrated in Figure 9(b).

To argue that the connected equilibrium in Figure 9(b) is a global minimizer one should rule out the existence of minimizers that have a form other than (66). In one dimension this was done via a simple explicit calculation; see Remark 3.2. Though such a simple argument does not seem to be available in two dimensions, we believe that the constant density in a disk is a global minimizer; for the problem in free space it was shown that such an equilibrium configuration is in fact a global attractor [10, 27].

4.2. Linear exogenous potential. Now we consider an exogenous gravitational potential $V(x_1, x_2) = gx_1$, with $g > 0$. The domain is the same as above, the half-plane $\Omega = [0, \infty) \times \mathbb{R}$, so the exogenous forces are acting (horizontally) toward the wall. Note that $\Delta V = 0$, and by

using this observation in (25) we infer that away from the wall the equilibrium densities are constant (equal to $2M$) on their support.

As in section 4.1, we search for equilibria in the form (66), which consist in a delta aggregation on the wall and a constant density free swarm. The same variables and setup from section 4.1 are being used here as well. In particular, the support $\Omega_{\bar{\rho}}$ of the equilibrium is given by (67), and mass conservation leads to (68). We solve numerically the necessary condition for equilibrium (70), with $\Lambda(\mathbf{x})$ given by

$$\begin{aligned}\Lambda(\mathbf{x}) = &\int_{-L}^{L}\left(-\frac{1}{2\pi}\ln\sqrt{x_1^2+(x_2-y_2)^2}+\frac{1}{2}\left(x_1^2+(x_2-y_2)^2\right)\right)f(y_2)dy_2\\ &+2M\iint_D\left(-\frac{1}{2\pi}\ln|\mathbf{x}-\mathbf{y}|+\frac{1}{2}|\mathbf{x}-\mathbf{y}|^2\right)\mathrm{d}\mathbf{y}+gx_1.\end{aligned}\tag{78}$$

Since the gravitational potential has zero Laplacian, by the same argument as in the zero gravity case one concludes that Λ is harmonic in D (see (72)). Consequently, the problem reduces to solving (73), with Λ given by (78). We solve this equation numerically to find approximations for L, d_1, d_2, and the profiles f and g of the wall aggregation and the free boundary.

As in one dimension, there is a critical value g_c such that for $g > g_c$ there is no equilibrium in the form (66). The gravity in this case is too strong and pins all mass on the boundary of the domain; the only equilibrium is a delta aggregation on the wall. For $g < g_c$, however, we find genuinely two-dimensional equilibria, which come in two types: connected and disconnected. In section 4.3 we show how g_c can be calculated in the two-dimensional problem. We find $g_c = f(0)/2$, where f is the density of the all-on-wall equilibrium (see (75) and Figure 9(a)). In our simulations with $M = 1$, $g_c \approx 0.564$. We now proceed to present the two cases separately.

Case $g < g_c$. Solutions to (73) of the form (66) exist only for mass ratios below a maximal value which we denote here by $\gamma(g)$. Recall that in one dimension, for subcritical gravities (note that in one dimension $g_c = M/2$), there exists a disconnected equilibrium for any mass ratio in the interval $(0, \sqrt{\frac{g_c}{g}} - 1)$, where the maximal mass ratio $\sqrt{\frac{g_c}{g}} - 1$ corresponds to the connected equilibrium (see Remark 3.3).

The subcritical gravity case in two dimensions parallels the findings in one dimension in the fact that for any fixed $g < g_c$, there exists a family of disconnected equilibria which approach, as the separation d_1 vanishes, a connected equilibrium supported on both the boundary and the interior of Ω. We parametrize this family of disconnected equilibria by r_M, the mass ratio defined in (74).

The major subtlety in two dimensions is that for low gravities, equilibria in the form (66) exist only for *certain* mass ratios in the interval $(0, \gamma(g))$. To illustrate this fact, we introduce a critical value $\tilde{g}_c$, with $\tilde{g}_c < g_c$ (as shown below, $\tilde{g}_c \approx 0.044$ for our simulations with $M = 1$). We find that for gravities $\tilde{g}_c < g < g_c$ there exists a disconnected equilibrium for *any* mass ratio in $(0, \gamma(g))$. On the other hand, for $g < \tilde{g}_c$, while solutions to (73) in the form (66) do exist for all $r_M \in (0, \gamma(g))$, not all of these solutions are equilibria. As a limiting case, we recover the findings from the zero gravity study, where none of the disconnected solutions to (73) were in fact equilibria. We now elaborate on these facts.

Remark 4.1 (critical gravities g_c and $\tilde{g}_c$). In one dimension it was trivial to find the critical

gravity $g_c = \frac{M}{2}$. In two dimensions, however, the calculation of g_c is not quite as trivial, and furthermore, a second critical gravity $\tilde{g}_c$ appeared during investigation. Provided that the wall profile f (see Figure 9(a)) satisfies some regularity conditions, we show in section 4.3 that $g_c = \frac{1}{2}f(0)$. As discussed above, $g > g_c$ is the case where gravity is so strong that it forces all mass onto the wall.

The other critical gravity, $\tilde{g}_c$, was found by numerical investigation. While no explicit formula was found for $\tilde{g}_c$, there is an intuitive understanding which is elaborated below when discussing Figure 12. The essential idea is that gravity is weak *and* there is just the right amount of mass off the wall so that it interacts strongly enough with the wall while remaining far enough that most of those interactions are attractive. For cases like this, mass begins leaving the wall near $(0, \pm L)$ since these points are farthest from the free swarm (the most attractive interaction).

(i) $\tilde{g}_c < g < g_c$.

Disconnected equilibria. For any fixed gravity $g \in (\tilde{g}_c, g_c)$, we find a family of disconnected solutions to (73) with mass ratios in the interval $(0, \gamma(g))$; as mentioned above, $\gamma(g)$ denotes the maximal value that the mass ratio of the two components can take for that particular g. In one dimension, $\gamma(g) = \sqrt{\frac{g_c}{g}} - 1$ can be calculated explicitly, as discussed in Remark 3.3. In two dimensions we approximate $\gamma(g)$ numerically; see Figure 3(b). Note that $\gamma(g)$ is strictly decreasing and touches zero at $g = g_c$. This is consistent with the fact that at larger gravities, less mass can end up in the free swarm, and the range of r_M decreases.

An illustration of a typical disconnected solution to (73) is shown in Figure 10(a); there $g = 0.064$. To check that these solutions are indeed equilibria, we compute numerically the velocity field at points on Ω_1, the part of the support that lies on the wall, and inspect its horizontal component (see Remark 2.2). Based on these investigations, we conclude that all the two-dimensional disconnected states we found here are indeed equilibria. Also, as in the one-dimensional case with subcritical gravity, these equilibria are *not* local minima for the energy, as (17) is not satisfied near the wall; see Figure 10(a) for a contour plot of Λ. Since $\Lambda(\mathbf{x})$ decreases from the wall to the free swarm, an infinitesimal perturbation of mass from the wall into $x_1 > 0$ would bring the mass into the free swarm.

To further illustrate the point above, we compute the energy corresponding to the disconnected steady states. Figure 10(c) shows the plot of the energy $E[\bar{\rho}]$ as a function of mass ratio r_M for $g = 0.064$; note that for this value of gravity, the maximal mass ratio is $\gamma(0.064) \approx 2.045$. We observe a monotonically decreasing profile that supports what has been noted above: Taking mass from the wall and placing it into $x_1 > 0$ would result dynamically in an equilibrium of larger mass ratio, which is more energetically favorable.

As the mass ratios of the disconnected equilibria increase toward the maximal value $\gamma(g)$, the free swarm gets closer and closer to the wall. This behavior is consistent with the results in one dimension, where explicit calculations show that the separation d_1 approaches zero in such limit. Numerical evidence suggests that at $r_M = \gamma(g)$, the two-dimensional free swarm touches the wall and forms a connected state. This aspect will be further discussed in the next paragraphs.

Connected equilibria. There exist two types of connected equilibria: one that corresponds to all mass on the wall ($r_M = 0$), and another that corresponds to the maximal mass ratio

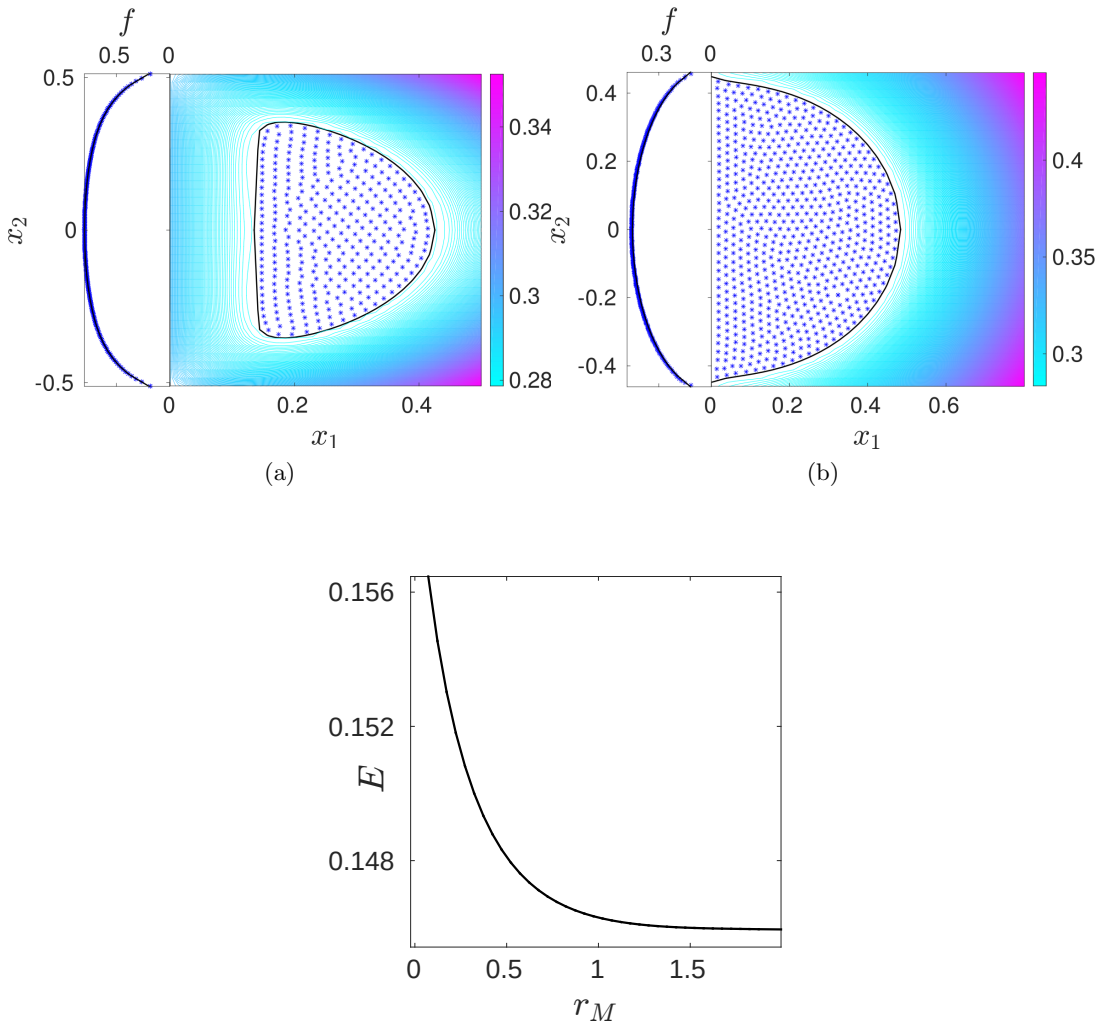

Figure 10. *Equilibria* (66) *on a half-plane for* $V(x_1, x_2) = gx_1$ *(linear exogenous potential) with* $g = 0.064$. (a) *Disconnected state consisting in a free swarm of constant density and a delta aggregation on the wall.* (b) *Connected state with a constant density in a domain adjacent to the wall and a delta aggregation on the wall. It should be mentioned that any apparent defects in* (a) *or* (b) *are the result of some numerical error and intrinsic error involving particles preferring to arrange in hexagons and the geometry of the free swarm not allowing hexagonal packing to cover the area.* (c) *Energy of equilibria* (66) *as a function of the mass ratio; the lowest energy state corresponds to the connected equilibrium with* $r_M = \gamma(g)$.

$r_M = \gamma(g)$. The first type can be obtained dynamically by initializing model (1) with a density that is supported entirely on the wall. In fact, since the gravitational forces vanish at the wall, the equilibrium density is identical to that computed in the zero gravity case; see equations (75)–(77) and Figure 9(a). The only distinction comes in checking the minimization condition

(14), which in the gravitational case reads as

$$\int_{-L}^{L}\left(-\frac{1}{2\pi}\ln\sqrt{x_1^2+(x_2-y_2)^2}+\frac{1}{2}\left(x_1^2+(x_2-y_2)^2\right)\right)f(y_2)dy_2+gx_1\geq\lambda \quad \text{for all } (x_1,x_2)\in\Omega_{\bar{\rho}}^c. \tag{79}$$

The gravitational term, gx_1, merely translates the minimum of $\Lambda(\mathbf{x})$ shown in Figure 9(a) toward the wall. This equilibrium is therefore not an energy minimizer until $g=g_c$, when the minimum of $\Lambda(\mathbf{x})$ becomes degenerate and $\Lambda(\mathbf{x})=\lambda$ for $\mathbf{x}\in\{0\}\times[-L,L]$.

The connected equilibria of the second type are supported on both the wall and the interior of Ω. As discussed above, they are realized when the free component of the disconnected state touches the wall in the limit $r_M\to\gamma(g)$. Alternatively, one can search for a connected state independently by assuming an equilibrium of the form (66), with a domain D that touches the wall ($d_1=0$). For this purpose we solved (13) numerically, with $\Lambda(\mathbf{x})$ given by (78). Figure 10(b) shows the connected equilibrium found by this direct approach for $g=0.064$, along with a particle simulation that has reached this steady state. Our numerical investigations indicate that there is a unique such connected equilibrium. Also, the connected state is a local minimizer of the energy, as can be inferred from the contour plot of Λ shown in the same figure. Based on our study (see, for instance, Figure 10(c)), we believe in fact that this equilibrium is a global minimizer of the energy, though for a definite conclusion one has to rule out the possibility of having minimizers of a more general form than (66); see Remark 3.2 for the one-dimensional case.

Figure 11 illustrates the idea that the connected equilibrium is obtained from the disconnected states upon touching the wall. The solid lines in Figures 11(a) and 11(b) show the boundary and the wall density profile f of the connected equilibrium, respectively, for the same value of g used above ($g=0.064$). The dashed lines correspond to the disconnected equilibrium with the largest mass ratio $r_M<\gamma(g)$ (or, equivalently, with the smallest separation $d_1>0$) that we were able to obtain in numerical simulations. The findings indicate that when the free swarm touches the wall at $r_M=\gamma(g)$, it establishes contact with the wall over an *entire* vertical segment, and not just at a single point. This suggests that there is a *continuous* deformation of the two-component equilibrium into the connected equilibrium of mass ratio $\gamma(g)$.

Finally, we remark that in our implementation for computing the connected equilibrium, we do not require $g(0)=L$; that is, we do not ask for the extent of the delta accumulation on the wall to match the boundary of the constant swarm in D. We assume instead the inequality $g(0)\leq L$, which allows the wall accumulation to extend beyond the points where the free boundaries $x_2=\pm g(x_1)$ meet the wall. And indeed, the equilibrium we find by solving (13) satisfies the *strict* inequality $g(0)<L$.

(ii) $g<\tilde{g}_c$. As in case (i), solutions to (73) of the form (66) exist for all mass ratios below a maximal value, which is denoted again by $\gamma(g)$. The profile of $\gamma(g)$ for $g\in(0,\tilde{g}_c)$ is shown in Figure 3(b); note that it connects smoothly at $g=\tilde{g}_c$, with $\gamma(g)$ computed as above for $g\in(\tilde{g}_c,g_c)$. Also, similarly to the one-dimensional case, $\gamma(g)$ approaches ∞ as $g\to 0$.

To check whether the computed solutions to (73) are indeed equilibria (see Remark 2.2), we inspect the velocity field on the wall. For an equilibrium, the velocities on the wall

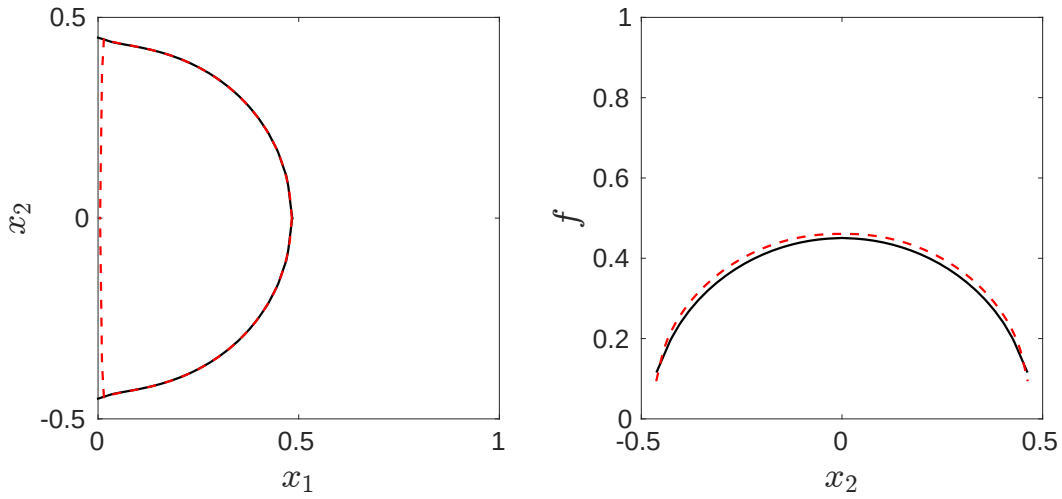

Figure 11. *Equilibria on a half-plane in two dimensions for $V(x_1, x_2) = gx_1$, with $g = 0.064$: The disconnected equilibria (66) approach a connected equilibrium state as the separation d_1 from the wall approaches 0 (or, equivalently, r_M approaches the maximal mass ratio $\gamma(g)$).* (a) *The solid line represents the connected solution of (66). The dashed line shows a disconnected equilibrium with a mass ratio $r_M = 1.873 < \gamma(g)$; this is the disconnected state with the largest mass ratio that we were able to obtain in our numerical investigations.* (b) *Profile f of the density on the wall corresponding to the connected (solid line) and disconnected (dashed line) equilibria shown in plot* (a).

(before applying the projection) should point *into* the wall or, equivalently, their horizontal components should be negative for all points in the support $[-L, L]$ of the wall density f. We find that there is an entire range of disconnected solutions to (73), with mass ratios $r_M \in (\alpha(g), \beta(g))$ (here $0 < \alpha(g) < \beta(g) < \gamma(g)$), which are *not* steady states. Alternatively, disconnected equilibria exist only for mass ratios $r_M \in (0, \alpha(g)) \cup (\beta(g), \gamma(g))$.

Figure 12 illustrates the idea above for $g = 0.04 < \tilde{g}_c$ and various mass ratios. At mass ratios $r_M \in (\alpha(g), \beta(g))$, the horizontal velocity is positive near the end of the wall profile (see curves labeled (3) and (4)). Hence, mass would leave the wall, and these solutions to (73) are not equilibria. For mass ratios outside this interval, the velocities are everywhere negative, and such solutions are indeed equilibria.

We approximate numerically $\alpha(g)$ and $\beta(g)$ and plot their profiles in Figure 3(b). Several observations can be inferred. First, the two profiles meet at $\tilde{g}_c$, indicating a bifurcation of saddle-node type in the qualitative behavior of solutions to (73). Second, the range $(\alpha(g), \beta(g))$ extends to $(0, \infty)$ in the limit $g \to 0$, which is consistent with the findings from the zero gravity case, i.e., no disconnected solution to (73) is a steady state. It is expected in fact that as g weakens, the free swarm components of the disconnected solutions tend to be farther from the wall, indicating more attractive forces on the wall profile near its ends. Additionally, weaker gravity means less force pushing toward the wall as well, accounting for the widening of the $(\alpha(g), \beta(g))$ region.

On the other hand, the equilibria with mass ratios $r_M \in (0, \alpha(g)) \cup (\beta(g), \gamma(g))$ have

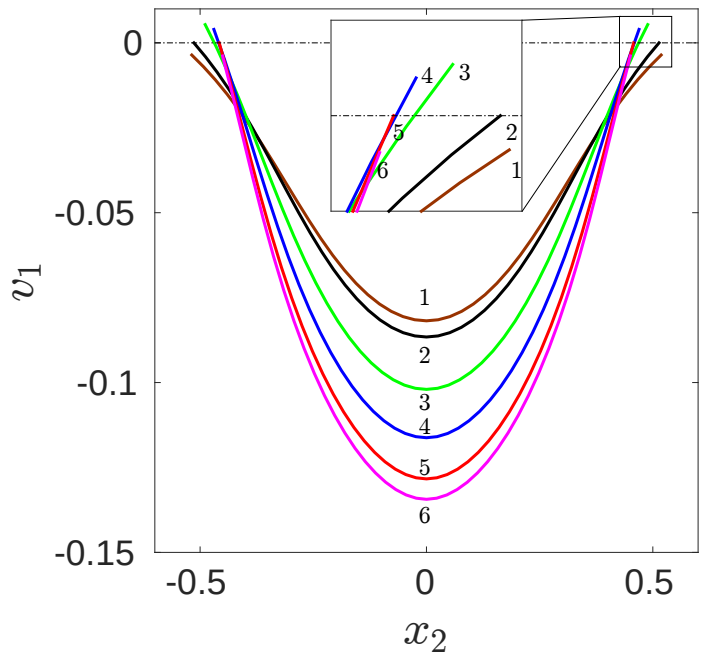

Figure 12. *Horizontal velocity (before taking the projection (3)) along wall profile of solutions to (73) for $g = 0.04 < \tilde{g}_c$ and (1) $r_M = 1.531$, (2) $r_M = \beta(g) \approx 1.379$, (3) $r_M = 1.078$, (4) $r_M = 0.744$, (5) $r_M = \alpha(g) \approx 0.439$, (6) $r_M = 0.362$. Note the positive velocities for $r_M \in (\alpha(g), \beta(g))$, that is, in (3) and (4), indicating that mass would leave the wall and thus these solutions are not steady states. See also Figure 3(b).*

properties similar to those found in case (i). Specifically, they are not local minimizers for the energy, and they approach a connected equilibrium, with support on both the wall and the interior of Ω, in the limit $r_M \to \gamma(g)$. The other connected equilibrium corresponds to the limit $r_M \to 0$ and represents an aggregation supported entirely on the wall. The profile of this wall equilibrium does not depend on the particular value of the gravity (see Figure 9(a)).

We confirmed all the findings above with particle simulations. In particular, we initialized the particle code at a disconnected state of form (66), with mass ratio in the range $(\alpha(g), \beta(g))$ and density support provided by the solutions to (73). We observed that indeed, such states are not equilibria, as particles near the end of the wall extent leave the wall and join the free swarm component.

Case $g > g_c$. The equilibrium in this case consists in a delta aggregation on the wall, of form (75), with mass constraint given by (76). As noted above, the exogenous potential V vanishes on the support $\Omega_{\bar{\rho}} = \{0\} \times [-L, L]$ of $\bar{\rho}$, and hence solving (13) is identical to the zero gravity case (see (77)). We find the same density profile f illustrated in Figure 9(a). By checking (79) one infers that this equilibrium is a local minimizer of the energy. We believe this to be a global minimizer, though we do not have a good argument for excluding other possible equilibrium configurations on the wall. Numerical simulations do support that it is a global minimizer in that we have not seen any other state that is reached dynamically.

4.3. Calculation of critical gravity g_c. To calculate the critical gravity g_c, we consider the equilibrium consisting of all mass on the wall; see (75) and Figure 9(a). We then pose the following question: How strong does gravity need to be such that a particle placed in the interior of Ω always feels a velocity toward the wall? We consider such a particle at position $(\epsilon, 0)$ with $\epsilon > 0$. We get from (2b) that the velocity in the horizontal direction felt by this particle is

$$v_1 = -\int_{-L}^{L} \left(1 - \left(2\pi(\epsilon^2 + x_2^2)\right)^{-1}\right) \epsilon f(x_2) dx_2 - g.$$

To study the competition between social and gravitational forces, one can focus just on the social velocity, defined by

$$v_1^s = -\int_{-L}^{L} \left(1 - \left(2\pi(\epsilon^2 + x_2^2)\right)^{-1}\right) \epsilon f(x_2) dx_2, \tag{80}$$

representing the velocity acting on the particle by interaction with the aggregation on the wall. With this notation, the horizontal velocity v_1 can be written as

$$v_1 = v_1^s - g. \tag{81}$$

We first investigate numerically which ϵ maximizes the social velocity. To that purpose, we take the approximation of the wall density profile $f(x_2)$ (see Figure 9(a)) and evaluate (80) for $\epsilon \in (0, 1]$. We do not evaluate directly at $\epsilon = 0$ because there is a discontinuity there as the particle ceases to feel any velocity in the horizontal direction once $\epsilon = 0$. We refer the reader to section 4.4 for details on how v_1^s is approximated.

The numerical investigation indicates that v_1^s is maximized in the limit as $\epsilon \to 0$; see Figure 13. To further cement this evidence, we note that this is expected, as repulsion (corresponding to positive velocity in this case) becomes stronger as distances shrink. Returning to the question we posed at the beginning, by (81), gravity is strong enough to yield negative horizontal velocity v_1, provided that g is larger than the maximal social velocity. Consequently, we set

$$g_c = \lim_{\epsilon \to 0} v_1^s. \tag{82}$$

In our simulations, an approximation of $\lim_{\epsilon \to 0} v_1^s$ can already be inferred from Figure 13. A more instructive and explicit formula can be derived, however, by taking the limit directly in (80):

$$\lim_{\epsilon \to 0} v_1^s = \lim_{\epsilon \to 0} \int_{-L}^{L} \left(2\pi(\epsilon^2 + x_2^2)\right)^{-1} \epsilon f(x_2) dx_2. \tag{83}$$

Assume that $f(x_2)$ has a convergent Taylor series centered on $x_2 = 0$:

$$f(x_2) = f(0) + \sum_{n=1}^{\infty} c_{2n} x_2^{2n}. \tag{84}$$

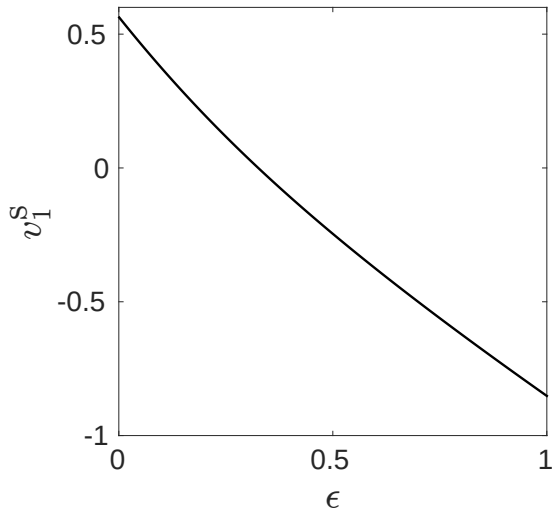

Figure 13. *Social velocity* (80) *acting from the aggregation on the wall (see* (75) *and Figure* 9(a)*) on a particle at position* $(\epsilon, 0)$.

Note that we have used here the symmetry of the wall profile about $x_2 = 0$. Equations (83) and (84) then give

$$\lim_{\epsilon\to 0} v_1^s = f(0) \lim_{\epsilon\to 0} \int_{-L}^{L} \frac{\epsilon}{2\pi(\epsilon^2 + x_2^2)} dx_2 + \lim_{\epsilon\to 0} \int_{-L}^{L} \sum_{n=1}^{\infty} \frac{\epsilon c_{2n} x_2^{2n}}{2\pi(\epsilon^2 + x_2^2)} dx_2. \tag{85}$$

Observe that

$$\begin{aligned} \left| \lim_{\epsilon\to 0} \epsilon \int_{-L}^{L} \sum_{n=1}^{\infty} \frac{c_{2n} x_2^{2n}}{2\pi(\epsilon^2 + x_2^2)} dx_2 \right| &\le \left| \lim_{\epsilon\to 0} \epsilon \int_{-L}^{L} \sum_{n=1}^{\infty} \frac{1}{2\pi} c_{2n} x_2^{2n-2} dx_2 \right| \\ &\le \frac{1}{2\pi} \left| \lim_{\epsilon\to 0} \epsilon \int_{-L}^{L} \sum_{n=1}^{\infty} 2n(2n-1) c_{2n} x_2^{2n-2} dx_2 \right| \\ &= 0, \end{aligned} \tag{86}$$

where we have assumed that $f''(x_2)$ has a convergent Taylor series as well.

Also, by an explicit calculation,

$$\lim_{\epsilon\to 0} \int_{-L}^{L} \frac{\epsilon}{2\pi(\epsilon^2 + x_2^2)} dx_2 = \frac{1}{2}. \tag{87}$$

With (85)–(87), (82) gives

$$g_c = \frac{1}{2} f(0). \tag{88}$$

Our numerical simulations yield $f(0) \approx 1.128$ (cf. Figure 9(a)), and hence we find $g_c \approx 0.564$. This value also agrees with Figure 13 (as it should).

4.4. Numerical implementations.

4.4.1. Particle method. Consider N particles with positions x_i and velocities v_i. In free space, the particle method for model (1) is simply implemented by numerically integrating

$$\frac{dx_i}{dt} = v_i, \tag{89a}$$

$$v_i = -\frac{M}{N}\sum_{j\neq i}\nabla K(x_i - x_j) - \nabla V(x_i), \tag{89b}$$

with $1 \leq i \leq N$.

In domains with boundaries, one needs to consider the possibility of a particle meeting the boundary within a time step. Let Δt denote the time step used in simulations, and for the sake of simplicity consider an explicit Euler method for time integration. If within a time step, particle i meets the boundary, then, in accordance with (2b) and (3), from the moment of collision it only continues to move in the tangential direction to the boundary.

For the one-dimensional problem on a half-line, this simply means that had a particle at x_i with velocity v_i reached the origin within a time step Δt, then it should simply be placed at the origin at the end of the time step. The resulting integrating scheme is then given by

$$x_i(t + \Delta t) = x_i(t) + \Delta t \bar{P}_{x_i} v_i(t), \tag{90}$$

where the projection operator $\bar{P}_{x_i}$, which generalizes (3), is given by

$$\bar{P}_{x_i} v_i = \begin{cases} v_i & \text{if } x_i + \Delta t v_i \geq 0, \\ -\Delta t^{-1} x_i & \text{otherwise.} \end{cases} \tag{91}$$

For the two-dimensional problem on a half-plane we should acknowledge that the vertical velocity of a particle remains unchanged upon colliding with the wall. In this case, a particle $x_i = (x_{i,1}, x_{i,2})$ with current velocity $v_i = (v_{i,1}, v_{i,2})$ updates its position according to (90), except that in two dimensions the discrete projection operator is

$$\bar{P}_{x_i} v_i = \begin{cases} (v_{i,1}, v_{i,2}) & \text{if } x_{i,1} + \Delta t v_{i,1} \geq 0, \\ (-\Delta t^{-1} x_{i,1}, v_{i,2}) & \text{otherwise.} \end{cases} \tag{92}$$

We used several general methods for getting disconnected states:

- using initial states that are highly concentrated (very small support) and very close (or adjacent) to the wall;
- (one dimenson) using initial states as in section 3.3.1 (in separated form) or as in section 3.3.2 (randomly generated from a uniform distribution on a segment in Ω);
- manually removing particles from the wall and placing them into the free swarm. This allows us to see representations of all disconnected equilibria even if they are not dynamically achievable.

Finally, we mention particular issues that can arise with regard to the choice of time step Δt. There are two phenomena that one can observe:

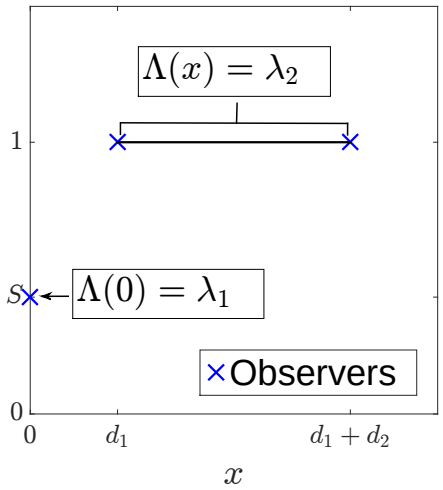

Figure 14. *Abstracted solution presumed in the numerical solver in one dimension showing locations of observers where we solve $\Lambda(x)$ to be a constant. Variables for the system are d_1, d_2, S, λ_1, and λ_2, as shown in the figure.*

- If particles are very concentrated and/or Δt is too large, then one can observe erratic dynamics where particles are sent far away from the free swarm.
- Related to the item above, particle methods applied in the manner described here tend to overapproximate the number of particles on the wall in their resultant states, though generally these errors are relatively small and we have mitigated the severity through decreasing the time step.

4.4.2. Discretization of the first variation of the energy ((28) and (73)).

One-dimensional case. We assume a solution of the form (26) where we now treat S, d_1, and d_2 as variables to be determined by satisfying (73). Furthermore, we also focus on the disconnected state, so λ_1, λ_2 are also variables. We use the term *observers* in this context to describe points along the boundary of $\Omega_{\bar{\rho}}$ at which we evaluate $\Lambda(x)$. In one dimension we require only three observers; see Figure 14. Finally, we consider the mass constraint (27) and the mass ratio (44); in general we keep r_M and M fixed.

Then our system of equations encompasses (27), (44), and

$$\Lambda(0) = \lambda_1, \quad \Lambda(d_1) = \lambda_2, \quad \Lambda(d_1 + d_2) = \lambda_2 \tag{93}$$

for a total of five equations for five unknowns. We also mention that if one fixes the mass ratio to be that of the minimizer for a given gravity g, then the result from solving the system of equations has $|\lambda_2 - \lambda_1|$ and d_1 below the tolerance of the solver, thus effectively recovering the connected solution.

Two-dimensional case: Disconnected. Because of the symmetry about $x_2 = 0$, we need only focus on half the space but can extend to the full space using symmetry. We now assume a solution of the form (66) where d_1, d_2, L, λ_1, λ_2, as well as the profiles $f(x_2)$ and $g(x_1)$ need

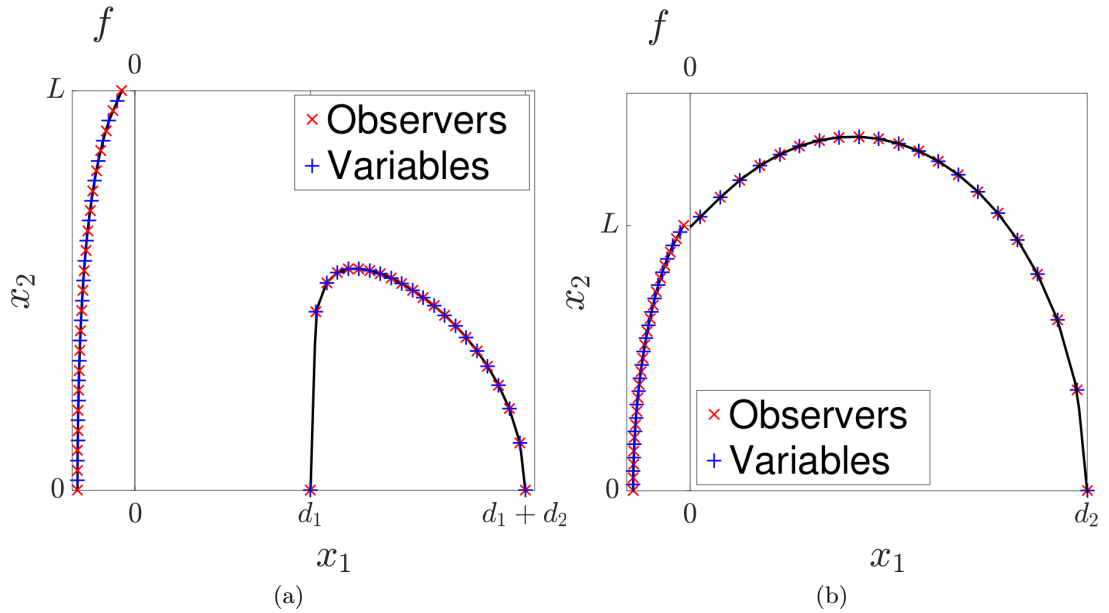

Figure 15. *Abstracted disconnected* (a) *and connected* (b) *solutions presumed in the numerical solver in two dimensions showing locations of observers where we solve* $\Lambda(x)$ *to be a constant. Variables for the system are* d_1, d_2, L, λ_1, λ_2, *and* $f(x_2)$ *and* $g(x_1)$ *evaluated on the numerical grid (see* (95)*).*

to be determined. We define equidistant vertical and horizontal grids

$$y_i = \frac{L}{N_f} i, \quad 0 \le i \le N_f, \qquad x_j = d_1 + \frac{d_2}{N_g} j, \quad 0 \le j \le N_g, \tag{94}$$

along with midpoints $y_i^* = \frac{1}{2}(y_{i-1} + y_i)$ for $1 \le i \le N_f$ and $x_j^* = \frac{1}{2}(x_{j-1} + x_j)$ for $1 \le j \le N_g$. We seek to find the $N_f + N_g$ variables

$$f(y_i^*) = f_i, \quad 1 \le i \le N_f, \qquad g(x_j^*) = g_j, \quad 1 \le j \le N_g. \tag{95}$$

The profile density f and the free boundary g are then extended with a linear interpolant.

To solve for (73) we use observers at $(0, y_i)$ for $0 \le i \le N_f$, (x_j^*, g_j) for $1 \le j \le N_g$, $(d_1, 0)$, and $(d_1 + d_2, 0)$; see Figure 15(a). We also have the mass condition (68) and the mass ratio condition (74). Together we have $N_f + N_g + 5$ conditions in total and $N_f + N_g + 5$ variables.

Two-dimensional case: Connected. The connected state implementation uses the same procedure in dealing with $f(x_2)$ but differs for the free boundary g. First, we lose the point $(d_1, 0)$ as $d_1 = 0$, and we do not pin this edge now. Second, we drop the mass ratio condition and now we only have λ as $\lambda_1 = \lambda_2 =: \lambda$. These are the only differences though, and we wind up with $N_f + N_g + 4$ conditions and $N_f + N_g + 4$ variables; see Figure 15(b).

The system of equations is solved with the MATLAB function `fsolve` using default settings, and integrals are evaluated with `integral` or `integral2` for one- or two-dimensional integration, respectively. When using `integral2` we use the iterated method setting.

Remark 4.2 (mass and mass ratio constraints). In one dimension the mass constraint (27) and the mass ratio constraint (44) are explicit, and we implement them directly in the numerics as additional conditions.

In two dimensions, recall that we work with the linear interpolants of f and g in which case, by using a numerical integrator, we can compute the necessary integrals for the mass condition (68) and mass ratio condition (74), namely

$$\int_{-L}^{L} f(x_2)dx_2 \quad \text{and} \quad |D| = \int_{d_1}^{d_1+d_2} \int_{-g(x_1)}^{g(x_1)} dx_2 dx_1.$$

Specifically, we used the MATLAB functions `integral` and `integral2` to do the numerical integration. In using `integral2` we employed the iterated method as described in the function's documentation.

5. Closing remarks and future directions. The present work has shown that the extensively studied aggregation model (1) has a potentially undesirable feature when posed in domains with boundaries: Solutions robustly evolve to equilibria which are not local minimizers of the energy. We illustrated this phenomenon in both one and two dimensions. In particular, in one dimension we took advantage of a reduced system by which we could track explicitly the evolution of the end points and center of mass of the free swarm (see (52)), and hence quantify the basin of attraction of disconnected (nonminimizer) equilibria.

The reduced dynamics in one dimension can also be used to understand the essential factor for why solutions in the presence of boundaries evolve into unstable minimizers: Once concentrations form on the boundary, there is no mechanism in the model to break them apart—note that in the reduced dynamics (51), the strength S of the delta aggregation at the boundary remains fixed through time evolution. Viewed from this perspective, the aggregation model seems flawed when boundaries are considered. To end the paper on a positive note and to open new directions for future research in this matter, we briefly present some of our preliminary investigations on how the aggregation model can be rectified.

Consider the aggregation model with quadratic nonlinear diffusion in a domain Ω:

$$\rho_t + \nabla \cdot (\rho v) = \nu \Delta(\rho^2), \tag{96}$$

with v given by (1b) and with no-flux boundary conditions prescribed on $\partial\Omega$. In principle, one could use an arbitrary power ρ^m, $m > 1$, for the nonlinear diffusion, but we illustrate the idea here only for $m = 2$. The diffusion coefficient $\nu > 0$ is taken to be small. We note that model (96) is also a gradient flow with respect to the energy (see also (5))

$$E_\nu[\rho] = \nu \int_\Omega \rho^2(x)\,\mathrm{d}x + \frac{1}{2}\int_\Omega \int_\Omega K(x-y)\rho(x)\rho(y)\,\mathrm{d}x\,\mathrm{d}y + \int_\Omega V(x)\rho(x)\,\mathrm{d}x. \tag{97}$$

The aggregation model with nonlinear diffusion has been considered by various works in recent years. Such works include variational studies [6], well-posedness of solutions [11], as well as investigations on equilibria and long time behavior of solutions [19, 13]; the latter works are particularly relevant to the present paper. Nevertheless, the approach we consider now is novel: Regard (96) as a *regularization* of the aggregation model (2), and show that

the above degeneracies of the aggregation model are corrected by adding a small amount of nonlinear diffusion.

One might ask why we do not consider linear diffusion, which could be easily implemented into a numerical scheme. The main concern here is the loss of compact solutions. With nonlinear diffusion as described above, we expect compact equilibria as found in [13]. Therefore we focus on nonlinear diffusion, as we simply wish to showcase a mechanism to stop the model from evolving into nonminimizing states.

To illustrate the regularization concept, we have computed numerical solutions of (96) using the finite-volume method developed in [15]. We note that this method has been specifically designed for aggregation models of this sort; in particular, the method preserves positivity of solutions as well as retaining a discrete gradient flow structure. It has been demonstrated in [15] that the method performs accurate computations of long time behavior and stationary states of model (96).

We present results in both one and two dimensions which support the idea that (96) is a meaningful regularization of (2). We denote below by $\rho_\nu(\mathbf{x}, t)$ the solutions of (96), and by $\bar{\rho}_\nu(\mathbf{x})$ its equilibria. The approach is to consider model (96) initialized near a disconnected (unstable) equilibrium of (2), and to contrast the nonminimizer equilibria achieved with model (2) with equilibria obtained with model (96).

In the context of the finite-volume discretization, a disconnected equilibrium of (2) can be approximated by placing mass S in cells adjacent to the wall. In one dimension this amounts to setting the density of the first cell adjacent to the wall equal to $\frac{S}{\Delta x}$, where Δx is the grid size. In two dimensions this amounts to considering the wall profile in Figure 10 and the cells adjacent to this profile. Then for each point along the wall profile we place that mass into the closest cell.

Figure 16(a) shows snapshots of the time evolution of $\rho_\nu(x, t)$ in one dimension, for $\nu = 10^{-4}$, in the absence of a gravitational potential ($V = 0$). As seen in the figure, the effect of adding small quadratic diffusion to (2) is that the model no longer evolves into a nonminimizer of the energy (such as the disconnected equilibrium in Figure 1(a)), but approaches instead a smoothed-out version of the (connected) energy minimizer of (2) shown in Figure 1(b). Figure 16(b) shows dynamically achieved equilibria of (96) for decreasing values of ν; as expected, the smaller the diffusion, the sharper the approximation of the connected equilibrium.

Figure 17 demonstrates that a similar regularization procedure occurs in the presence of a gravitational potential (here $g = 0.125$, as we had without diffusion). Initialized at an unstable equilibrium of model (2) (Figure 2(a)), model (96) evolves dynamically into an approximation of the connected equilibrium from Figure 2(b). Note that by the effect of diffusion, delta concentrations at the boundary have now been replaced by steep boundary layers of large (but finite) amplitude.

Finally, Figure 18 shows the regularization phenomenon in two dimensions with gravity ($g = 0.064$, as for the numerical experiments without diffusion). Note that we do not consider the case $g = 0$ here, as in the absence of gravity, model (2) in two dimensions does not lead to disconnected equilibria. Figure 18 demonstrates that model (96) initialized at an unstable (disconnected) equilibrium of (2) (Figure 18(a)) evolves into an approximation of the connected energy minimizer (Figure 18(b)); here $\nu = 10^{-4}$.

As an additional numerical check, for both one and two dimensions with gravity, we

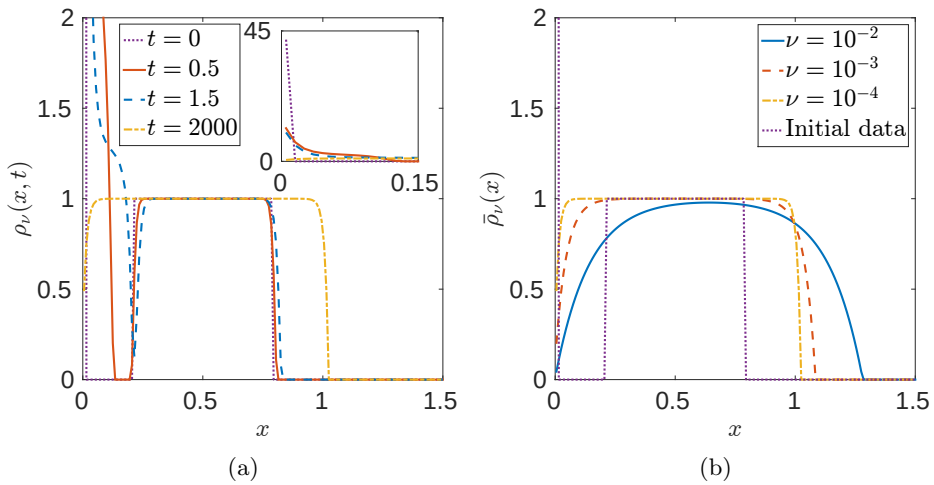

Figure 16. *Aggregation model with nonlinear diffusion on a half-line for $V = 0$ (no exogenous potential). Initialized near a (disconnected) nonminimizer equilibrium of model (2) (see Figure 1(a)), solutions to (96) approach asymptotically a smoothed-out version of the (connected) minimizer equilibrium of (2) shown in Figure 1(b). (a) Several time snapshots of $\rho_\nu(x,t)$ for $\nu = 10^{-4}$, with a zoom-out near the boundary shown in insert. (b) Equilibria of (96) for various values of ν. The smaller the diffusion coefficient, the sharper the approximation of the connected equilibrium.*

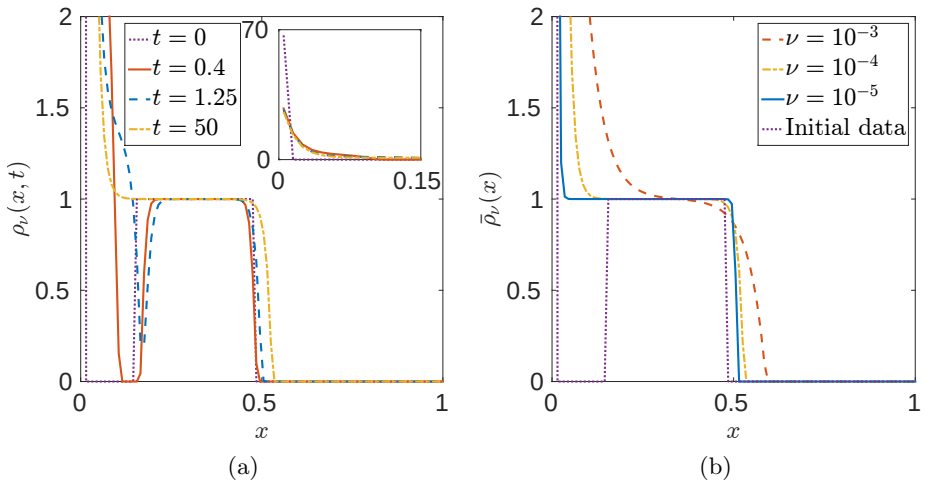

Figure 17. *Aggregation model with nonlinear diffusion on a half-line for $V(x) = gx$ with $g = 0.125$. Solutions to (96) are initialized near a (disconnected) nonminimizer equilibrium of model (2) (see Figure 2(a)). In contrast to the evolution governed by model (2), solutions to (96) evolve dynamically into an approximation of the connected minimizer from Figure 2(b). (a) Several time snapshots of $\rho_\nu(x,t)$ for $\nu = 10^{-4}$; the insert shows a zoom-out near the boundary. Note that although the final time here is much smaller than in Figure 16(a), in both figures the states were evolved until the flux at any location was below 10^{-12}. (b) Equilibria of (96) for various values of ν. By nonlinear diffusion, delta concentrations at the origin have been replaced by boundary layers of finite amplitude. Approximations to the connected equilibrium become sharper with decreasing ν.*

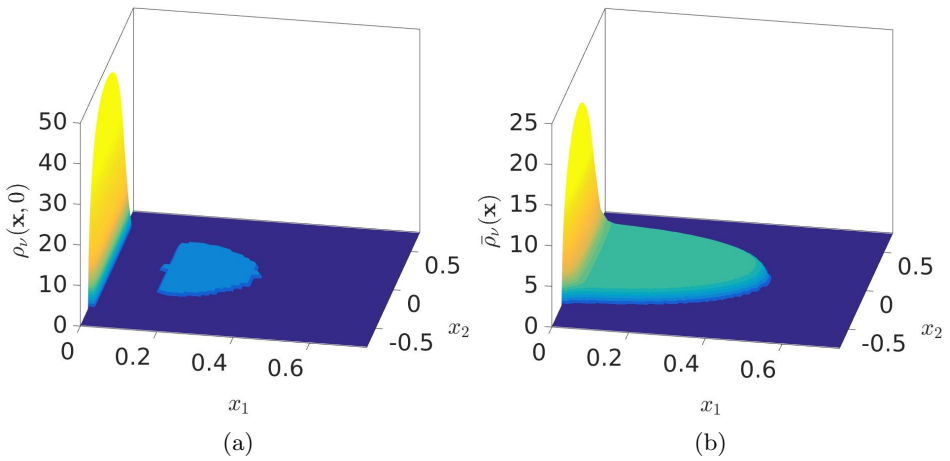

Figure 18. *Aggregation model with nonlinear diffusion on a half-plane with* $\nu = 10^{-4}$ *in two dimensions for* $V(x_1, x_2) = gx_1$ *with* $g = 0.064$. (a) *Solutions to* (96) *are initialized at an unstable (disconnected) equilibrium of* (2) *(see Figure* 10(a)*).* (b) *Solutions to* (96) *reach asymptotically a connected equilibrium, representing an approximation of the connected energy minimizer for* (2) *shown in Figure* 10(b).

computed the mass contained in the boundary layer near the wall and compared it with the mass of the Dirac delta accumulation *on* the wall for the model with no diffusion. In one dimension, we computed the total mass of densities greater than $M = 1$, which we regard as the mass in the boundary layer. We found that the mass in the boundary layer approaches $\frac{1}{2}$ as ν decreases to zero, supporting the claim that solutions ρ_ν of (96) approach asymptotically the connected equilibrium of (2) (note that for $g = 0.125$, the connected equilibrium of (2) has a Dirac delta accumulation of strength $S = \frac{1}{2}$ at the origin). In two dimensions we computed the total mass of densities greater than $2M = 2$ along horizontal lines $x_2 = \text{const.}$, which we interpret as the vertical distribution of mass in the boundary layer. In support of the regularization thesis, we found that such distribution of mass approaches, as ν decreases, the wall profile $f(x_2)$ of the connected equilibrium shown in Figure 10(b).

In conclusion, adding small nonlinear diffusion to the model allows concentrations to break apart and, hence, provides a mechanism that prevents the model from evolving into a nonminimizer of the energy. A rigorous study of the zero diffusion limit of solutions $\rho_\nu(x,t)$ to (96), and of minimizers to (97), as well as a more systematic numerical investigation of the diffusion model, are currently being considered by the authors and will be reported in a future publication.

6. Appendix. We provide below the six equations derived from (64). The four equations that ensure $\Lambda(x) = \lambda_2$ for $x \in [d_1, d_1 + d_2]$ are

$$\frac{C}{L^{-2}+\mu^2}\exp\left(\frac{d_1}{L}\right)\left(-\frac{1}{L}\cos(\mu d_1) - \mu\sin(\mu d_1)\right)$$
$$+\frac{D}{L^{-2}+\mu^2}\exp\left(\frac{d_1}{L}\right)\left(-\frac{1}{L}\sin(\mu d_1) + \mu\cos(\mu d_1)\right) + \frac{L\lambda_2}{\epsilon}\exp\left(\frac{d_1}{L}\right) + S = 0,$$

$$\frac{C}{1+\mu^2}\exp(d_1)\Big(-\cos(\mu d_1)-\mu\sin(\mu d_1)\Big)$$
$$+\frac{D}{1+\mu^2}\exp(d_1)\Big(-\sin(\mu d_1)+\mu\cos(\mu d_1)\Big)+\frac{\lambda_2}{\epsilon}\exp(d_1)+S=0,$$
$$\frac{C}{L^{-2}+\mu^2}\exp\left(-\frac{d_1+d_2}{L}\right)\Big(-\frac{1}{L}\cos(\mu(d_1+d_2))+\mu\sin(\mu(d_1+d_2))\Big)$$
$$+\frac{D}{L^{-2}+\mu^2}\exp\left(-\frac{d_1+d_2}{L}\right)\Big(-\frac{1}{L}\sin(\mu(d_1+d_2))-\mu\cos(\mu(d_1+d_2))\Big)$$
$$+\frac{L\lambda_2}{\epsilon}\exp\left(\frac{-(d_1+d_2)}{L}\right)=0,$$
$$\frac{C}{1+\mu^2}\exp(-(d_1+d_2))\Big(-\cos(\mu(d_1+d_2))+\mu\sin(\mu(d_1+d_2))\Big)$$
$$+\frac{D}{1+\mu^2}\exp(-(d_1+d_2))\Big(-\sin(\mu(d_1+d_2))-\mu\cos(\mu(d_1+d_2))\Big)+\frac{\lambda_2}{\epsilon}\exp(-(d_1+d_2))=0.$$

The equation that ensures $\Lambda(0)=\lambda_1$ is

$$-GL\Bigg(\frac{C}{L^{-2}+\mu^2}\exp\Big(-\frac{y}{L}\Big)\Big(-\frac{1}{L}\cos(\mu y)+\mu\sin(\mu y)\Big)$$
$$+\frac{D}{L^{-2}+\mu^2}\exp\Big(-\frac{y}{L}\Big)\Big(-\frac{1}{L}\sin(\mu y)-\mu\cos(\mu y)\Big)+\frac{L\lambda_2}{\epsilon}\exp\Big(-\frac{y}{L}\Big)\Bigg)\Bigg|_{y=d_1}^{y=d_1+d_2}$$
$$+\Bigg(\frac{C}{1+\mu^2}\exp(-y)\Big(-\cos(\mu y)+\mu\sin(\mu y)\Big)$$
$$+\frac{D}{1+\mu^2}\exp(-y)\Big(-\sin(\mu y)-\mu\cos(\mu y)\Big)+\frac{\lambda_2}{\epsilon}\exp(-y)\Bigg)\Bigg|_{y=d_1}^{y=d_1+d_2}+S(1-GL)=\lambda_1.$$

Finally, the mass constraint equation gives

$$S+\frac{C}{\mu}(\sin(\mu(d_1+d_2))-\sin(\mu d_1))-\frac{D}{\mu}(\cos(\mu(d_1+d_2))-\cos(\mu d_1))-\frac{\lambda_2 d_2}{\epsilon}=M.$$

Acknowledgment. The authors would also like to acknowledge valuable suggestions from the anonymous referees, in particular, the recommendation to include a forward-looking conclusion section.

REFERENCES

[1] L. Ambrosio, N. Gigli, and G. Savaré, *Gradient Flows in Metric Spaces and in the Space of Probability Measures*, Lectures Math. ETH Zürich, Birkhäuser Verlag, Basel, 2005.

[2] D. Balagué, J. A. Carrillo, T. Laurent, and G. Raoul, *Dimensionality of local minimizers of the interaction energy*, Arch. Ration. Mech. Anal., 209 (2013), pp. 1055–1088.

[3] D. Balagué, J. A. Carrillo, T. Laurent, and G. Raoul, *Nonlocal interactions by repulsive-attractive potentials: Radial ins/stability*, Phys. D, 260 (2013), pp. 5–25.

[4] J. M. Ball, *Dynamic energy minimization and phase transformations in solids*, in ICIAM 91 (Washington, DC, 1991), SIAM, Philadelphia, 1992, pp. 3–14.
[5] J. M. Ball, P. J. Holmes, R. D. James, R. L. Pego, and P. J. Swart, *On the dynamics of fine structure*, J. Nonlinear Sci., 1 (1991), pp. 17–70.
[6] J. Bedrossian, *Global minimizers for free energies of subcritical aggregation equations with degenerate diffusion*, Appl. Math. Lett., 24 (2011), pp. 1927–1932.
[7] A. J. Bernoff and C. M. Topaz, *A primer of swarm equilibria*, SIAM J. Appl. Dyn. Syst., 10 (2011), pp. 212–250, https://doi.org/10.1137/100804504.
[8] A. L. Bertozzi, J. A. Carrillo, and T. Laurent, *Blow-up in multidimensional aggregation equations with mildly singular interaction kernels*, Nonlinearity, 22 (2009), pp. 683–710.
[9] A. L. Bertozzi and T. Laurent, *Finite-time blow-up of solutions of an aggregation equation in* $\mathbf{R}^n$, Comm. Math. Phys., 274 (2007), pp. 717–735.
[10] A. L. Bertozzi, T. Laurent, and L. Flavien, *Aggregation and spreading via the Newtonian potential: The dynamics of patch solutions*, Math. Models Methods Appl. Sci., 22 (2012), 1140005.
[11] A. L. Bertozzi and D. Slepčev, *Existence and uniqueness of solutions to an aggregation equation with degenerate diffusion*, Commun. Pure Appl. Anal., 9 (2010), pp. 1617–1637.
[12] M. Bodnar and J. J. L. Velazquez, *An integro-differential equation arising as a limit of individual cell-based models*, J. Differential Equations, 222 (2006), pp. 341–380.
[13] M. Burger, R. Fetecau, and Y. Huang, *Stationary states and asymptotic behavior of aggregation models with nonlinear local repulsion*, SIAM J. Appl. Dyn. Syst., 13 (2014), pp. 397–424, https://doi.org/10.1137/130923786.
[14] J. A. Cañizo, J. A. Carrillo, and F. S. Patacchini, *Existence of compactly supported global minimisers for the interaction energy*, Arch. Ration. Mech. Anal., 217 (2015), pp. 1197–1217.
[15] J. A. Carrillo, A. Chertock, and Y. Huang, *A finite-volume method for nonlinear nonlocal equations with a gradient flow structure*, Commun. Comput. Phys., 17 (2015), pp. 233–258.
[16] J. A. Carrillo, M. DiFrancesco, A. Figalli, T. Laurent, and D. Slepčev, *Global-in-time weak measure solutions and finite-time aggregation for nonlocal interaction equations*, Duke Math. J., 156 (2011), pp. 229–271.
[17] J. A. Carrillo, R. J. McCann, and C. Villani, *Contractions in the 2-Wasserstein length space and thermalization of granular media*, Arch. Ration. Mech. Anal., 179 (2006), pp. 217–263.
[18] J. A. Carrillo, D. Slepčev, and L. Wu, *Nonlocal-interaction equations on uniformly prox-regular sets*, Discrete Contin. Dyn. Syst., 36 (2016), pp. 1209–1247.
[19] L. Chayes, I. Kim, and Y. Yao, *An aggregation equation with degenerate diffusion: Qualitative property of solutions*, SIAM J. Math. Anal., 45 (2013), pp. 2995–3018, https://doi.org/10.1137/120874965.
[20] R. Choksi, R. C. Fetecau, and I. Topaloglu, *On minimizers of interaction functionals with competing attractive and repulsive potentials*, Ann. Inst. H. Poincaré Anal. Non Linéaire, 32 (2015), pp. 1283–1305.
[21] J. Cortés, *Discontinuous dynamical systems: A tutorial on solutions, nonsmooth analysis, and stability*, IEEE Control Syst. Mag., 28 (2008), pp. 36–73.
[22] Q. Du and P. Zhang, *Existence of weak solutions to some vortex density models*, SIAM J. Math. Anal., 34 (2003), pp. 1279–1299, https://doi.org/10.1137/S0036141002408009.
[23] W. E, *Dynamics of vortex liquids in Ginzburg-Landau theories with applications to superconductivity*, Phys. Rev. B, 50 (1994), pp. 1126–1135.
[24] L. C. Evans, *Partial Differential Equations*, 2nd ed., Grad. Stud. Math. 19, American Mathematical Society, Providence, RI, 2010.
[25] K. Fellner and G. Raoul, *Stable stationary states of non-local interaction equations*, Math. Models Methods Appl. Sci., 20 (2010), pp. 2267–2291.
[26] R. C. Fetecau and Y. Huang, *Equilibria of biological aggregations with nonlocal repulsive-attractive interactions*, Phys. D, 260 (2013), pp. 49–64.
[27] R. C. Fetecau, Y. Huang, and T. Kolokolnikov, *Swarm dynamics and equilibria for a nonlocal aggregation model*, Nonlinearity, 24 (2011), pp. 2681–2716.
[28] A. F. Filippov, *Differential Equations with Discontinuous Righthand Sides*, Math. Appl. (Soviet Ser.) 18, Kluwer Academic Publishers, Dordrecht, The Netherlands, 1988 (translated from the Russian).
[29] J. M. Haile, *Molecular Dynamics Simulation: Elementary Methods*, John Wiley & Sons, New York, 1992.

[30] D. D. Holm and V. Putkaradze, *Aggregation of finite-size particles with variable mobility*, Phys. Rev. Lett., 95 (2005), 226106.
[31] D. D. Holm and V. Putkaradze, *Formation of clumps and patches in self-aggregation of finite-size particles*, Phys. D., 220 (2006), pp. 183–196.
[32] Y. Huang and A. L. Bertozzi, *Self-similar blowup solutions to an aggregation equation in R^n*, SIAM J. Appl. Math., 70 (2010), pp. 2582–2603, https://doi.org/10.1137/090774495.
[33] B. D. Hughes and K. Fellner, *Continuum models of cohesive stochastic swarms: The effect of motility on aggregation patterns*, Phys. D, 260 (2013), pp. 26–48.
[34] T. Kolokolnikov, H. Sun, D. Uminsky, and A. L. Bertozzi, *Stability of ring patterns arising from two-dimensional particle interactions*, Phys. Rev. E, 84 (2011), 015203(R).
[35] A. J. Leverentz, C. M. Topaz, and A. J. Bernoff, *Asymptotic dynamics of attractive-repulsive swarms*, SIAM J. Appl. Dyn. Syst., 8 (2009), pp. 880–908, https://doi.org/10.1137/090749037.
[36] A. Mogilner and L. Edelstein-Keshet, *A non-local model for a swarm*, J. Math. Biol., 38 (1999), pp. 534–570.
[37] S. Motsch and E. Tadmor, *Heterophilious dynamics enhances consensus*, SIAM Rev., 56 (2014), pp. 577–621, https://doi.org/10.1137/120901866.
[38] R. Simione, D. Slepčev, and I. Topaloglu, *Existence of ground states of nonlocal-interaction energies*, J. Stat. Phys., 159 (2015), pp. 972–986.
[39] I. H. Sloan and A. Spence, *The Galerkin method for integral equations of the first kind with logarithmic kernel: Theory*, IMA J. Numer. Anal., 8 (1988), pp. 105–122.
[40] P. J. Swart and P. J. Holmes, *Energy minimization and the formation of microstructure in dynamic anti-plane shear*, Arch. Rational Mech. Anal., 121 (1992), pp. 37–85.
[41] C. M. Topaz, A. L. Bertozzi, and M. A. Lewis, *A nonlocal continuum model for biological aggregation*, Bull. Math. Biol., 68 (2006), pp. 1601–1623.
[42] C. M. Topaz, M. R. D'Orsogna, L. Edelstein-Keshet, and A. J. Bernoff, *Locust dynamics: Behavioral phase change and swarming*, PLoS Comput. Biol., 8 (2012), e1002642.
[43] G. Toscani, *One-dimensional kinetic models of granular flows*, M2AN Math. Model. Numer. Anal., 34 (2000), pp. 1277–1291.
[44] L. Wu and D. Slepčev, *Nonlocal interaction equations in environments with heterogeneities and boundaries*, Comm. Partial Differential Equations, 40 (2015), pp. 1241–1281.
[45] Y. Yan and I. H. Sloan, *On integral equations of the first kind with logarithmic kernels*, J. Integral Equations Appl., 1 (1988), pp. 549–579.